Materials Today Communications 35 (2023) 105984

Contents lists available at ScienceDirect

Materials Today Communications

journal homepage: www.elsevier.com/locate/mtcomm

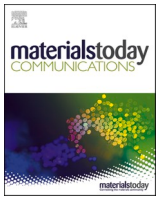

Impact of borosilicate bioactive glass scaffold processing and reactivity on in-vitro dissolution properties

Agata Szczodra [a,*,1], Jenna M. Tainio [a,1], Amel Houaoui [a], Hongfei Liu [a], Juuso Pohjola [a], Susanna Miettinen [a,b], Delia S. Brauer [c], Jonathan Massera [a]

[a] Tampere University, Faculty of Medicine and Health Technology, Tampere, Finland
[b] Research, Development and Innovation Centre, Tampere University Hospital, Tampere, Finland
[c] Otto-Schott-Institut, Friedrich-Schiller-Universität, Jena, Germany

ARTICLE INFO

Keywords:
Borosilicate bioactive glasses
Scaffolds
In vitro dissolution
3D printing
Human cells

ABSTRACT

In this study, bulk borosilicate glasses and 3D scaffolds (processed by the burn-off technique and by robocasting) were synthesized to investigate the impact of the manufacturing method, glass composition and preincubation time on in vitro dissolution and cell response. The studied compositions are based on commercial bioactive glass S53P4 (BonAlive) where 12.5% SiO_2 has been replaced by B_2O (labelled B12.5), and part of the CaO is replaced with MgO and SrO (labelled B12.5-Mg-Sr). First, the impact of the processing and glass composition, on the dissolution rate, was assessed. As expected, scaffolds were found to exhibit faster dissolution, due to the increased surface area, when compared to the bulk glass. Furthermore, the 3D printed scaffolds were found to dissolve faster than the burn-off scaffolds. Moreover, scaffolds made from B12.5-Mg-Sr glass composition exhibited slower ion release and precipitation of calcium phosphate (CaP) layer, when compared to B12.5, due to the stabilizing effect of Mg and Sr. Finally, dynamic condition produces lower ion releases that static condition and could be more optimal for in vitro cell growth. Secondly, in culture with murine MC3T3-E1 cells, it was shown that 3 days preincubation would be optimal to decrease the burst of ions that is known to lead to cell death. However, it was found that MC3T3-E1 survived and proliferated only in presence of B12.5-Mg-Sr scaffolds. Finally, it was shown that despite scaffolds having different porosities, they had no significant difference on human adipose-derived stem cells (hADSCs) survival. This manuscript brings new information on 1) the impact of material design (porosity) and composition on dissolution kinetic sand reactivity, 2) the impact of static vs dynamic testing on in-vitro dissolution and 3) the impact of materials' pre-incubation on cell behavior.

1. Introduction

Current BAG bone substitutes are limited to powders, granules, and putties. No porous 3D scaffolds are currently commercialized. Indeed, commercial silicate BAG e.g., S53P4 demonstrate crystallization tendencies during sintering, thus inhibiting the processing of porous construct [1-4]. For 3D scaffold to be osteoconductive, large pores (50–500 μm) and highly interconnected porosity (> 50 μm) with overall porosity over 50% are needed to allow tissue infiltration and regeneration [5,6]. Additionally, it is crucial for proper bone repair that scaffold would provide mechanical support, with properties close to the natural bone [5,7].

To overcome the high crystallization tendency of traditional silicate bioactive glasses, borosilicate glasses were developed [4,8]. High boron content was found efficient in producing glasses with fast and more complete conversion into hydroxyapatite and with thermal properties allowing sintering into 3D scaffolds without crystallization [9,10,4,8]. However, high porosity of porous scaffolds, and fast dissolution of borosilicate glasses lead to extensive ion release, in vitro, often resulting in cells death [11,12]. However, this is not a problem in vivo where ions get constantly flushed away [4,13]. Consequently, it is difficult to evaluate the true potential of borosilicate 3D porous scaffolds as bone replacement based on in vitro studies. Thus, understanding how different parameters can affect ion release and dissolution rate, would allow for better control over their final performance in vitro and easier translation into in vivo and clinical studies.

* Corresponding author.
E-mail address: agata.szczodra@tuni.fi (A. Szczodra).
[1] Shared authorship.

https://doi.org/10.1016/j.mtcomm.2023.105984
Received 20 October 2022; Received in revised form 30 March 2023; Accepted 11 April 2023
Available online 11 April 2023

Table 1
Nominal glass composition (%).

Glass	mol%						
	SiO_2	B_2O_3	CaO	Na_2O	P_2O_5	MgO	SrO
B12.5	47.12	6.73	21.77	22.66	1.72	0	0
B12.5-Mg-Sr	47.12	6.73	6.77	22.66	1.72	5	10

To gain better understanding on the impact of borosilicate glass composition and porosity on the in-vitro dissolution and cell behaviour, two borosilicate glasses based on the S53P4 composition were developed; B12.5: 47.12 SiO_2–6.73 B_2O_3–21.77 CaO–22.66 Na_2O–1.72 P_2O_5 (mol%) and B12.5-Mg-Sr: 47.12 SiO_2–6.73 B_2O_3–6.77 CaO–22.66 Na_2O–1.72 P_2O_5–5 MgO–10 SrO (mol%). In the study by Tainio et al. the initial characterization of B12.5 glasses modified, where Mg and/or Sr where partially substituted for Ca, has been done [14]. Based on the results, the B12.5 and B12.5-Mg-Sr glass compositions, with respectively fastest and slowest dissolution rate, were chosen for this study. The idea was 1) to assess which aqueous solution better mimics the dissolution/reaction of bioactive glasses in culture medium, 2) to assess if an increased pre-incubation time can decrease the initial burst release, of a fast degrading bioactive glass, while maintaining a significant release of therapeutic ions, 3) to better understand the changes in ion release when the dissolution is in dynamic rather than static, 4) to study the impact of scaffolds structure on the release of ions, and 5) assess the impact of ions release and pre-incubation time on cell behavior.

Generally, the replacement of CaO with SrO and/or MgO has stabilizing effect on borate network and helps to reduce the dissolution rate of the glass [14]. Moreover, substitution of SrO and/or MgO for CaO increases the hot forming domain in S53P4, thus allows better sinterability with suppressed crystallization tendencies [15,16]. Additionally, SrO has been shown to stimulate an osteogenic response from hBMSCs [17,18] and MC3T3-E1 (J. [19]; [20]. Furthermore, Sr was reported to promote the proliferation and differentiation of osteoblasts [21-23]. Magnesium is also essential for bone development and homeostasis, and it has been shown to stimulate osteogenesis in human osteoblasts [24, 25]. Furthermore, addition of MgO and SrO in the composition of the glass promotes bone repair and remodeling [26-28].

Moreover, due to improved thermal properties, these glass compositions were used to produce 3D porous scaffolds using the porogen burn-off or 3D printing (robocasting) manufacturing methods. Porogen burn-off is a relatively easy technique that does not require advanced or expensive equipment. The porogen burn-off also allows fabrication of scaffolds with high porosity (>90%) and macropores having dimension up to 500 μm [29,30]. However, this technique usually leads to low pore interconnectivity with, often, interconnection too small to favour cell migration. [29,31]. 3D printing technique allows a precise control over the object structures such as the interconnectivity, shape, orientation, and pore size which can be customized through a 'layer-by-layer' manufacturing [29,32,33]. Computer-aided-design (CAD) is used and allows the development of fully interconnected porous networks that cannot be easily built using conventional techniques.

Finally, an effect of manufacturing method and glass composition on static/dynamic in vitro dissolution in TRIS and SBF was studied by Inductively Coupled Plasma – Optical Emission Spectroscopy (ICP-OES) and SEM. The effect of glass composition and preincubation time in TRIS and αMEM culture medium on murine MC3T3-E1 cell response was also investigated. Lastly, effect of manufacturing method on hADSCs cell behaviour was examined. Moreover, scaffolds mechanical properties were investigated as well as their microstructure analyzed by micro-computed tomography (μCT).

The goal of this study was to show that the control over the glass composition, preincubation time and manufacturing method can prevent excessive ion release from borosilicate 3D porous scaffolds and consequently improve bioactivity and cell viability. Moreover, we introduced borosilicate 3D scaffolds with different porosities as a suitable candidate for bone tissue engineering. The studied scaffolds are promising as bone grafts that promote, support, and direct the new bone growth. Moreover, 3D printed scaffolds could allow manufacturing of custom-made implants with tailored porosity.

2. Materials and methods

2.1. Preparation of bioactive glass powders

B12.5 and B12.5-Mg-Sr were prepared from analytical grade (Na_2CO_3, NH_4H_2PO4, $(CaHPO_4)(2(H_2O))$, $CaCO_3$, MgO, $SrCO_3$, H_3BO_3 (Sigma Aldrich, St Louis, MO, USA), and Belgian quartz sand. The 60 g batches of B12.5 and B12.5-Mg-Sr were melted for 30 min at 1300 °C in a platinum crucible in LHT 02/17 LB Speed electric furnace (Nabertherm GmbH, Lilienthal, Germany) in air atmosphere. The batch was heated from room temperature to 800 °C using 10 °C/min heating rate and kept at 800 °C for 15 min to allow evaporation of volatile CO_2. Then the temperature was raised from 800 °C to 1300 °C using 10 °C/min heating rate and kept at 1300 °C for 30 min to homogenize the glass melt. The molten glasses were casted and then annealed for at least 6 h at 450 °C in electric muffle furnace (Nabertherm L 3/12). After annealing, glasses at room temperature were crushed, milled in a planetary ball mill (Fritsch GmbH, Idar-Oberstein, Germany), and sieved into less than 38 μm particles with sieves (Gilson Company, Inc., Ohio, USA). The nominal oxide compositions of the glasses are given in Table 1.

2.2. Scaffold manufacturing

Burn-off scaffolds were made by pressing mixture of glass powder and porogen inside a cylindrical mold. The ammonium bicarbonate, NH_4HCO_3 (Sigma-Aldrich, 99.5%, CAS No. 1066–33–7), was used as the porogen (70 vol%) and mixed with glass (30 vol%). The porogen is assumed to fully evaporate during the sintering, leaving pores behind.

3D printed scaffolds were made by robocasting using 3Dn-Tabletop printer (nScrypt Inc., Orlando, Florida, USA), and controlled via the Machine Tool 3.0 system software.

Firstly, the Pluronic solution, which acts as the binder, was made by mixing the Pluronic 127 (Sigma-Aldrich, CAS No. 9003–11–6) and distilled water in the ratio of 25:75 wt% respectively, in an ice bath, until the solution turned clear. The solution was then stored at 4 °C.

Secondly, the ink was made by mixing glass powder and Pluronic solution in the ratio of 30:70 wt% respectively, using Vibrofix VF1 electrical shaker (IKA®-Labortechnic, Staufen, Germany) at 2500 rpm. Mixing was done in intervals of 30 s mixing and then 30 s cooling in the ice bath. The mixing-cooling cycles were repeated at least 5 times until the ink was homogenous and no bubbles could be visually seen. The ink was loaded into Optimum® 3cc printing cartridge (Nordson EFD, Bedfordshire, England) and left for 1 h at room temperature to achieve right viscosity for 3D printing.

Finally, the cartridge was attached to the 3D printer and ink extruded through the SmoothFlow Tapered Tips with tip diameter of 0.41 mm (Nordson EFD Optimum® SmoothFlow™, Westlake, Ohio, USA) onto the acrylic sheets (Folex AG, Seewen, Switzerland). The material feed was set to 18.0–22.0 psi, to maintain a continuous flow during movement of the tip. After drying at room temperature for at least 24 h to reduce the risk of collapse, scaffolds were ready for sintering.

For cellular experiments, the burn-off scaffolds and 3D printed scaffolds were compared to the bulk of these same glasses. Bulk scaffolds were made by pressing the glass powder into a cylindrical mold with diameter and height of 5 mm. The compacted pellets were placed onto a ceramic plate for the sintering.

Bulk, burn-off and 3D printed scaffolds were sintered for 1 h at between 540 and 545 °C (Nabertherm LT 9/11/SKM electric muffle furnace) in an air atmosphere. Sintering allows fusing of glass particles, but also removes the porogen and binder from scaffolds. The sintering

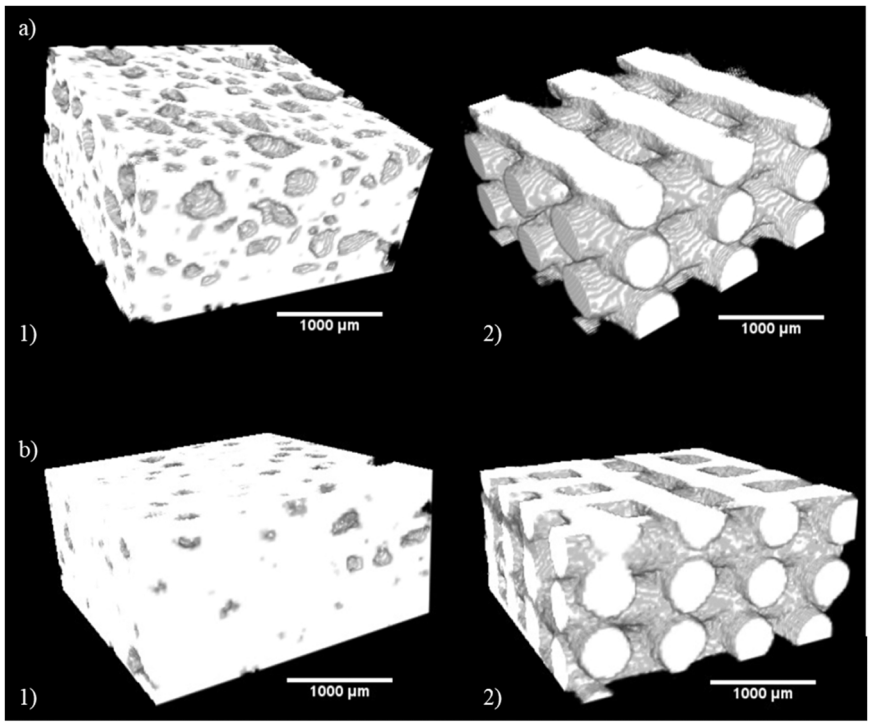

Fig. 1. 3D structure of scaffolds produced via 1) burn-off, 2) 3D printing of a a) B12.5, b) B12.5-Mg-Sr compositions.

Table 2
Average sizes of scaffolds used for static in vitro dissolution in TRIS and SBF.

	Burn-off		3D printed	
Type of scaffolds	Bottom diameter (mm)	Height (mm)	Bottom diameter (mm)	Height (mm)
B12.5	14.37 ± 0.16	4.3 ± 0.3	9.82 ± 0.17	4.45 ± 0.08
B12.5-Mg-Sr	12.59 ± 0.28	4 ± 0.39	8.41 ± 0.26	3.83 ± 0.11

process had three phases: 1) from room temperature to 300 °C at 1 °C/min, 2) from 300 °C to the sintering temperature at 5 °C/min and 3) staying at the sintering temperature for 1 h. Multistep, slow sintering is done to avoid sudden shrinkage which might cause cracking of the scaffolds. Sintered scaffolds were taken out after furnace cools down to room temperature and stored in a desiccator. Figure S1, presents the images of the produced scaffolds, post-sintering.

2.3. Material characterization

2.3.1. Porosity measurements

The estimation of the scaffolds' porosity was performed assuming that scaffolds are cylinder-shaped. The porosity was estimated using the following equation:

$$Porosity = (1 - \rho/\rho_0) \times 100\% \quad (1)$$

where the ρ_0 was the bulk density, and ρ was the apparent density (scaffolds mass divided by scaffold volume) of each scaffold. The porosities were obtained from at least 50 parallel samples per each glass composition and type and expressed as mean ± standard deviation (SD).

2.3.2. Micro-computed tomography (μCT)

Micro-computed tomography (μCT) was utilized to gain information about the scaffold 3D structures and these are shown in Fig. 1. Measurements were conducted with MicroXCT-400 (Carl Zeiss X-ray Microscopy, Inc., Pleasanton, California, USA) by having 80 kV tube voltage and 0.4x objective. The resulting pixel size was 16.7 μm. Scaffold structures were constructed from the obtained data with ImageJ software combined with 3D Viewer plugin. Images show that scaffolds produced via porogen burn-off had randomly sized and located round pores. 3D printed scaffolds were comprised of parallel filaments with constant spacing making interconnected porosity.

2.3.3. X-ray powder diffraction (XRD)

To evaluate if the 3D printed and porogen burn-off glass scaffolds stayed amorphous after sintering they were grounded to fine powder in a mortar and analyzed with a X-ray diffractometer (XRD). Measurements were conducted in the 10–60° 2θ diffraction angle range with MiniFlex™ (Rikagu, Tokyo, Japan).

2.3.4. Mechanical properties

Scaffolds produced via porogen burn-off had shrunk inhomogeneously during sintering. Thus, their top and bottom surfaces were ground flat with grit P800 SiC paper in Ethanol (96%, VWR Chemicals, CAS No. 64–17–5). Ground samples were dried overnight in a type B 8133 drying oven (Termaks, Bergen, Norway) at 37 °C.

For measurements burn-off and 3D printed scaffolds with diameter d≈ 11–14 mm and height h≈ 5–6 mm were used. Compression testing was conducted with Instron 4411 mechanical tester (Instron, Massachusetts, USA) by using a 0.5 mm/min deformation speed. 5 kN load cell was used for glass scaffolds. Highest compression values were taken from individual measurements to describe the compressive strength of glass scaffolds. The measurements were obtained from three parallel samples for each scaffold type and glass composition and expressed as mean ± standard deviation (SD).

2.3.5. Physico-chemical characterization

To study the dissolution behavior of the scaffolds and their bioactivity, they were immersed in in Tris(hydroxymethyl)aminomethane (TRIS) and Simulated Body Fluid (SBF), respectively. The average sizes of the scaffolds used for this characterization step are presented Table 2.

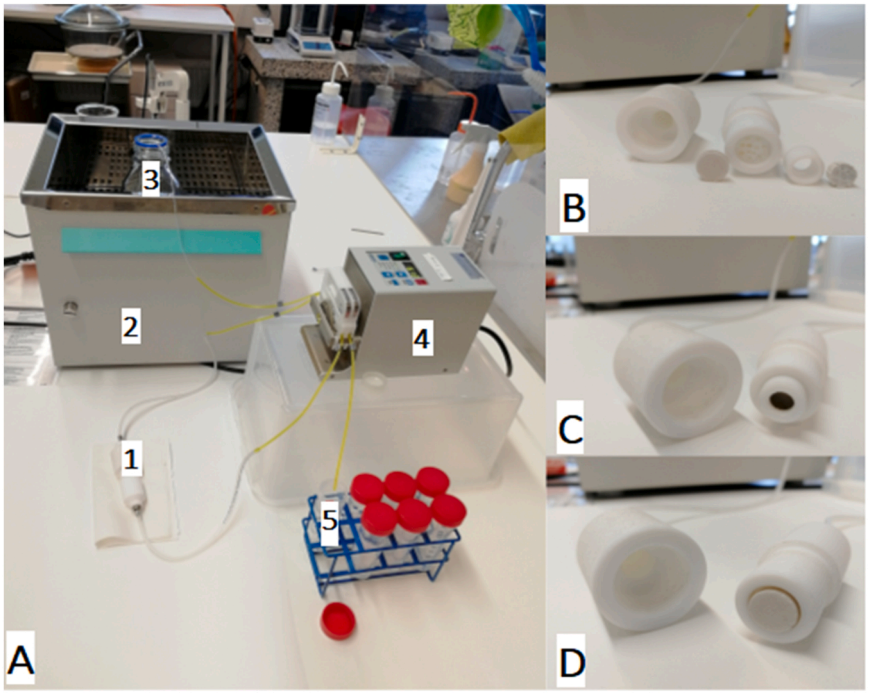

Fig. 2. Picture of the flow-through system. A) is the intact system: 1-reactor, 2-water bath, 3-bottle of SBF, 4-pump, 5-outflow; B is inner structure of reactor; C is a scaffold adjusted by a Teflon ring; D is a scaffold loaded into chamber.

2.3.6. Fourier transformation infrared spectroscopy (FTIR)

Sintered B12.5 and B12.5-Mg-Sr glass scaffolds were crushed into powders. FTIR measurements were conducted with a Spectrum One FTIR Spectrophotometer (PerkinElmer Inc., Massachusetts, USA) using the attenuated total reflectance (ATR) mode. 8 scan accumulations were performed in the 650–4000 cm^{-1} wavenumber range with a 4 cm^{-1} resolution. The spectra were baseline corrected and normalized to the peak with the highest intensity.

2.3.7. Dissolution in TRIS in static conditions

Dissolution of the scaffolds in TRIS was done to test the ions leaching, while the risk of ionic supersaturation was limited [34]. TRIS solution (50 mM) was prepared by mixing ultrapure TRIS (Sigma Aldrich, St Louis, MO, USA) and TRIS-HCl (Sigma Aldrich, St Louis, MO, USA) in pure water. The pH of the solution was adjusted to 7.4 at 37 °C. The solution was not refreshed over the course of the immersion test.

Burn-off and 3D printed scaffolds made from B12.5 and B12.5-Mg-Sr glass compositions were immersed in TRIS solution for up to 2 weeks in an incubator at 37 °C (Orbital incubator SI600, Stuart) with an orbital speed of 100 rpm. The volume of TRIS was calculated to maintain a mass/volume ratio constant at 20 mg/ml. At each timepoint (6, 24, 48, 72, 168, and 336 h), the pH of the immersion solution was measured at 37 °C using a S47-K SevenMultiTM pH-meter (Mettler-Toledo LLC, Ohio, USA). The ionic concentration was studied by Inductively Coupled Plasma – Optical Emission Spectroscopy (ICP-OES). After drying the samples 48 h at 37 °C, the mass loss ratio was calculated following the equation:

$$Massloss = (W_0 - W_t)/W_0 * 100 \quad (2)$$

Where the W_0 is the original mass before immersion, and W_t is the dry mass after each time of immersion.

This study was conducted on three parallel samples and two parallel blank samples, and the results are presented as mean ± SD.

2.3.8. Dissolution in SBF in static conditions

The samples in vitro bioactivity, related to the formation of HA and the change in ionic concentration, was studied in SBF, developed by Kokubo et al. and prepared following the methodology from the standard ISO/FDIS 23317. During the experiment, the solution was not refreshed to observe the precipitation of CaP.

Burn-off and 3D printed scaffolds made from B12.5 and B12.5-Mg-Sr glass compositions were immersed in SBF in the same way as TRIS immersion. The volume of SBF was calculated to maintain a mass/volume ratio constant at 20 mg/ml. At each timepoint (6, 24, 48, 72, 168, and 336 h), the pH of the solution was measured at 37 °C, the mass loss was calculated, and the ionic concentration was studied. This study was conducted on three parallel samples and two parallel blank samples, and the results are presented as mean ± SD.

2.3.9. Scanning electron microscope (SEM)

To assess the bioactivity and HA layer formation, SEM/EDX imaging was used to analyze scaffolds after 336 h of static immersion in SBF. For SEM analysis, the scaffold pieces were mounted in epoxy resin and polished with Struers Tegramin-30 automatic polishing machine up to 1 μm diamond suspension. Samples were carbon coated prior to analysis. Magnification of 250x, 15 kV acceleration voltage and back-scattered electrons were used for imaging. Thicknesses of the surface layers were obtained via image analysis with ImageJ from 10 different spots and the results are presented as mean ± SD.

2.3.10. Dissolution in SBF in dynamic conditions

The dynamic dissolution of burn-off and 3D printed scaffolds made from B12.5 and B12.5-Mg-Sr glass compositions, was evaluated in SBF with a flow-through system. Each scaffold was loaded separately in a home-made reactor, which was connected to the bottle of SBF solution on one end (inlet) and the outlet to tubes to collect the fluid. There was a detachable Teflon ring to adjust the cross-section of the reactor to match the size of the different type of scaffolds. The experiment for each sample was performed with SBF at 37 °C and at 0.4 ml/min flow rate for 74 h. At each timepoint, the pH of the outflow solution was measured, the outflow tube was removed and replaced with new container. For first three days the solution was collected 8 times per day during an 8-hour window. On the last day, the solution was collected 3 times during a

Table 3
Average porosity of scaffolds.

	Porosity (%)		
Type of scaffolds	Bulk	Burn-off	3D printed
B12.5	30.85 ± 8.53	72.5 ± 1.4	69.68 ± 3.19
B12.5-Mg-Sr	15.17 ± 7.38	60.4 ± 2.75	51.79 ± 5.77

Table 4
Average width and length of pores found in 3D printed scaffolds. Measured by optical microscope.

Type of scaffolds	Width (μm)	Length (μm)
B12.5 3D printed	280 ± 70	290 ± 60
B12.5-Mg-Sr 3D printed	192 ± 46	208 ± 57

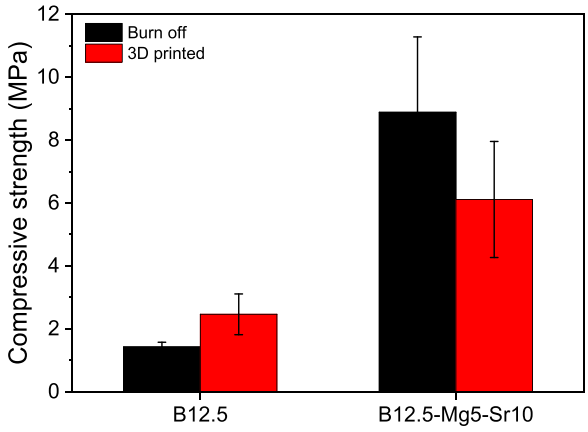

Fig. 3. Compressive strength at failure.

3-hour time window. The whole set-up is shown in Fig. 2. The analyses were conducted once on each sample and blank sample.

2.3.11. ICP analysis

The immersion solutions collected from static and dynamic in vitro dissolution in TRIS and SBF were diluted 10 times in 1 M high purity nitric acid for ion analysis. ICP-OES (Agilent technologies 5110, Santa Clara, CA, USA) was employed to quantify P^{3-} ($\lambda = 213.618$ nm), Ca^{2+} ($\lambda = 422.673$ nm), Mg^{2+} ($\lambda = 285.213$ nm), Si^{4+} ($\lambda = 250.690$ nm), B^{3+} ($\lambda = 249.772$ nm), Sr^{2+} ($\lambda = 421.552$ nm), and Na^{+} ($\lambda = 588.995$ nm) ion concentrations in the immersion solutions.

2.4. Effect of preincubation in TRIS and αMEM

Bulk, burn-off and 3D printed scaffolds with diameter d≈ 4.5 mm and height h≈ 4.5 mm, were immersed in TRIS and α-Minimum Essential Media (α-MEM) to investigate which preincubation time affects the ion release from the scaffolds.

One scaffold per each composition, scaffold type and timepoint, was immersed in TRIS solution for up to 6 days at 37 °C in incubator with an orbital speed of 100 rpm. The TRIS was refreshed at days 2 and 4 to mimic the changing of cell culture media. At each timepoint (day 1, 2, 4 and 6) and before refreshing, the samples for ICP measurement were collected and diluted 10 times in 1 M high purity nitric acid. Moreover, at each timepoint the pH of preincubation solution was measured. Because some samples were refreshed, the ICP and pH measurements of TRIS solution were conducted on one to three parallel samples and on one to three parallel blank samples, and the results are presented as mean ± SD.

Each scaffold, after immersion in TRIS, was immersed in α-Minimum Essential Media (α-MEM) (Gibco, Life Technologies, Carlsbad, CA, USA) containing glutamine supplemented with 1% penicillin/streptomycin (Gibco, Life Technologies, Carlsbad, CA, USA). After 24 h, preincubation solution was collected and diluted 10 times in 1 M high purity nitric acid. The ICP measurement of α-MEM were conducted once on each sample and once on blank sample.

Ion concentrations in collected TRIS and α-MEM preincubation solutions were measured as described in ICP analysis section. Scaffolds were removed from immersion solution, rinsed with ethanol and dried for 24 h before their mass was weighted. The volume of TRIS and α-MEM used for preincubation was calculated to maintain a mass/V ratio constant at 10 mg/ml.

2.5. Cell analysis with MC3T3-E1 and hADSCs

2.5.1. MC3T3-E1 and hADSCs expansion

Murine calvarial pre-osteoblastic MC3T3-E1 cells subclone four (ATCC, Manassas, VA, USA) were cultured in α-Minimum Essential Media (Gibco, Life Technologies, Carlsbad, CA, USA) containing glutamine supplemented with 10% Fetal Bovine Serum (FBS, Biosera, Marikina, Philippines) and 1% penicillin/streptomycin (Gibco, Life Technologies, Carlsbad, CA, USA). These, cells were used for initial evaluation and to develop a methodology.

Human ADSCs were isolated from subcutaneous abdominal tissue sample obtained from a female donor (age 49 years, BMI 21.4) at the Tampere University Hospital Department of Plastic Surgery with the donor's written informed consent and processed under ethical approval of the Ethics Committee of the Expert Responsibility area of Tampere University Hospital (R15161). The cells were isolated as described previously [35]. These cells, show greater translational potential which make them more clinically relevant compared to animal derived cells.

The mesenchymal origin of ADSCs was confirmed by surface marker expression analysis with flow cytometry [36] and ability of adipogenic and osteogenic differentiation [37] by Oil Red O and Alizarin Red staining, respectively. The cells were characterized as MSCs due to positive expression of CD73 (97%), CD90 (99%), and CD105 (99%), and low or negative expression of CD14 (1%), CD19 (0.6%), CD45 (2.6%), CD34 (8%) and HLA-DR (0.9%) [38,39] as well as accumulation of lipid droplets by Oil Red O and mineralized matrix deposition by Alizarin Red staining.

Human adipose-derived stem cells (hADSCs) were cultured in α-Minimum Essential Media (α-MEM) (Gibco, Life Technologies, Carlsbad, CA, USA) without nucleosides supplemented with 5% human serum (Serana Europe, Germany GmbH) and 1% penicillin/streptomycin (Gibco, Life Technologies, Carlsbad, CA, USA).

Both types of cells were cultured at 37 °C in a humidified atmosphere of 5% CO_2 balanced 95% air in incubator (Thermo Scientific forma stericycle i160 CO_2) until they reached over 80% confluence.

2.5.2. Preincubation of scaffolds before cell culturing

For this part of experiment scaffolds with average diameter of with height h= 4.2 ± 0.4 mm and diameter d= 4.4 ± 0.3 mm were used.

For cell tests with MC3T3-E1 cells, bulk B12.5 and B12.5-Mg-Sr scaffolds, were preincubated for either 1 or 6 days in TRIS always followed by 24 h in αMEM in incubator at 37 °C.

For cell test with hADSCs, bulk, burn-off and 3D printed scaffolds made from B12.5-Mg-Sr glass composition were preincubated for 2 days in TRIS and followed by 24 h in αMEM in incubator at 37 °C. For this test, only B12.5-Mg-Sr glass was studied. Each condition (bulk, burn-off, 3D printed) was studied in triplicate. Then, scaffolds were preincubated for 2 days in TRIS, followed by 24 h in αMEM in incubator at 37 °C. The volume of TRIS and α-MEM used for preincubation was calculated to maintain a mass/V ratio constant at 10 mg/ml. All scaffolds were sterilized for 3 h at 200 °C before preincubation.

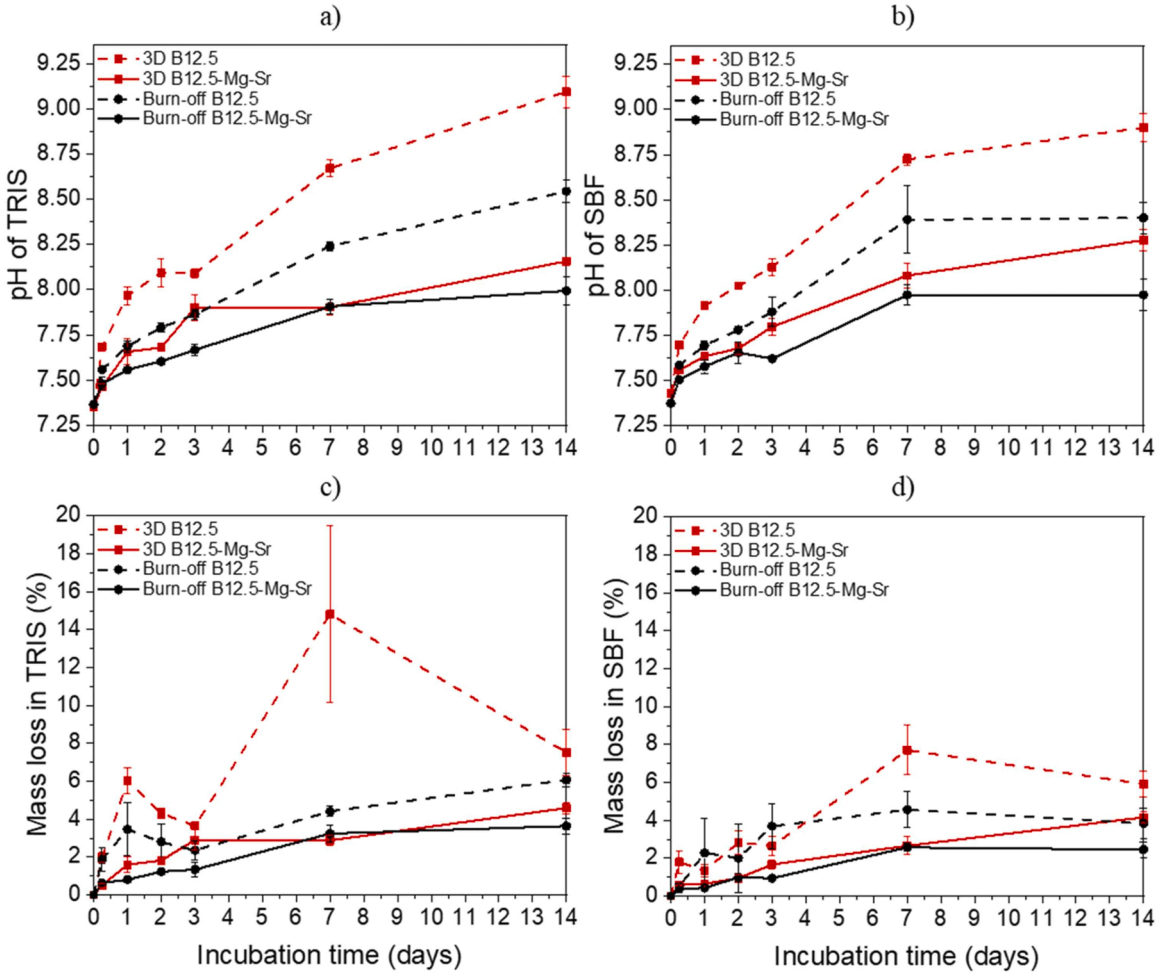

Fig. 4. a-b) pH of TRIS and SBF after static in vitro dissolution of scaffolds up to 14 days, c-d) mass loss of scaffolds after static in vitro dissolution in TRIS and SBF for up to 14 days.

2.5.3. Live/dead assay

Live/dead assay was used to detect cell viability in the proximity of the scaffolds and their dissolution by-products. Firstly, preincubated scaffolds were placed into 48 well plates (Thermo Scientific). For experiment with MC3T3-E1, 20.000 cells, passage 26–27 were seeded in 550 µl of α-MEM culture medium (containing glutamine, 10% FBS, 1% P/S) and cultured in contact with scaffolds for 24 h.

For cell experiments with hADSCs, 25.000 cells, passage 4 were seeded in 1 ml of α-MEM culture medium (no glutamine, 5% human serum, 1% P/S) and cultured in contact with scaffolds for 1, 3 and 7 days.

For both live/dead experiments, the positive control used was the Tissue Culture Polystyrene (TCPS) 48-wellplate seeded with cells, without scaffold.

At each timepoint, the cell culture media was collected and diluted 10 times in ultrapure water for ICP analysis. ICP measurements were conducted on three parallel samples and one blank sample and expressed as mean ± standard deviation (SD).

Next, wells with scaffolds were rinsed using Dulbecco's Phosphate Buffered Saline, DPBS (Gibco, Life Technologies, Carlsbad, CA, USA) heated to 37 °C. The staining solution was prepared according to the Live & Dead Kit (Live/Dead Cell Double Staining Kit, SIGMA-ALDRICH, 04511), added to the wells and incubated for 30 mins at room temperature. Viable and necrotic MC3T3-E1 and ASCs cells were stained with 1% (v/v) of Calcein AM and 0,5% (v/v) Ethidium homodimer-1 solution. Finally, wells with scaffolds were rinsed with DPBS and cells were observed under the fluorescence microscope Olympus IX51 (Olympus Corporation, Japan).

3. Results and discussion

3.1. Characterization of the materials

3.1.1. Porosity

3D scaffolds with large pores (50–500 µm) and porosity between 50% and 90% are necessary for scaffold to be osteoconductive and allow tissue infiltration and regeneration crucial for proper bone tissue engineering [5,7]. Also, it is crucial that the scaffolds remain amorphous post-sintering. Table 3 present the overall porosity of the produced scaffolds (Eq.1) while Figure S2, presents the XRD diffraction pattern of the scaffold post sintering. From XRD analysis it is clear that no noticeable diffraction peaks can be noticed, indicating that the scaffolds remain amorphous. Regardless of the technique used, the porosities of B12.5 scaffolds were higher than that of B12.5-Mg-Sr scaffolds. This could be explained by enhanced sinterability of B12.5-Mg-Sr BAGs caused by addition of Mg and Sr [14,16]. Moreover, the porogen burn-off method can produce scaffolds with higher porosity compared to those produced by the 3D printing method, depending on design. While the ratio between glass particles and porogen was tailored to obtain similar porosity between the two techniques, one might expect that the size distribution and interconnection between pores will be lower in the case of the burn-off scaffolds when compared to scaffolds obtained by robocasting [29]. Most importantly, the scaffolds had porosity over 50% which is in line with the recommendation for tissue and cell migration

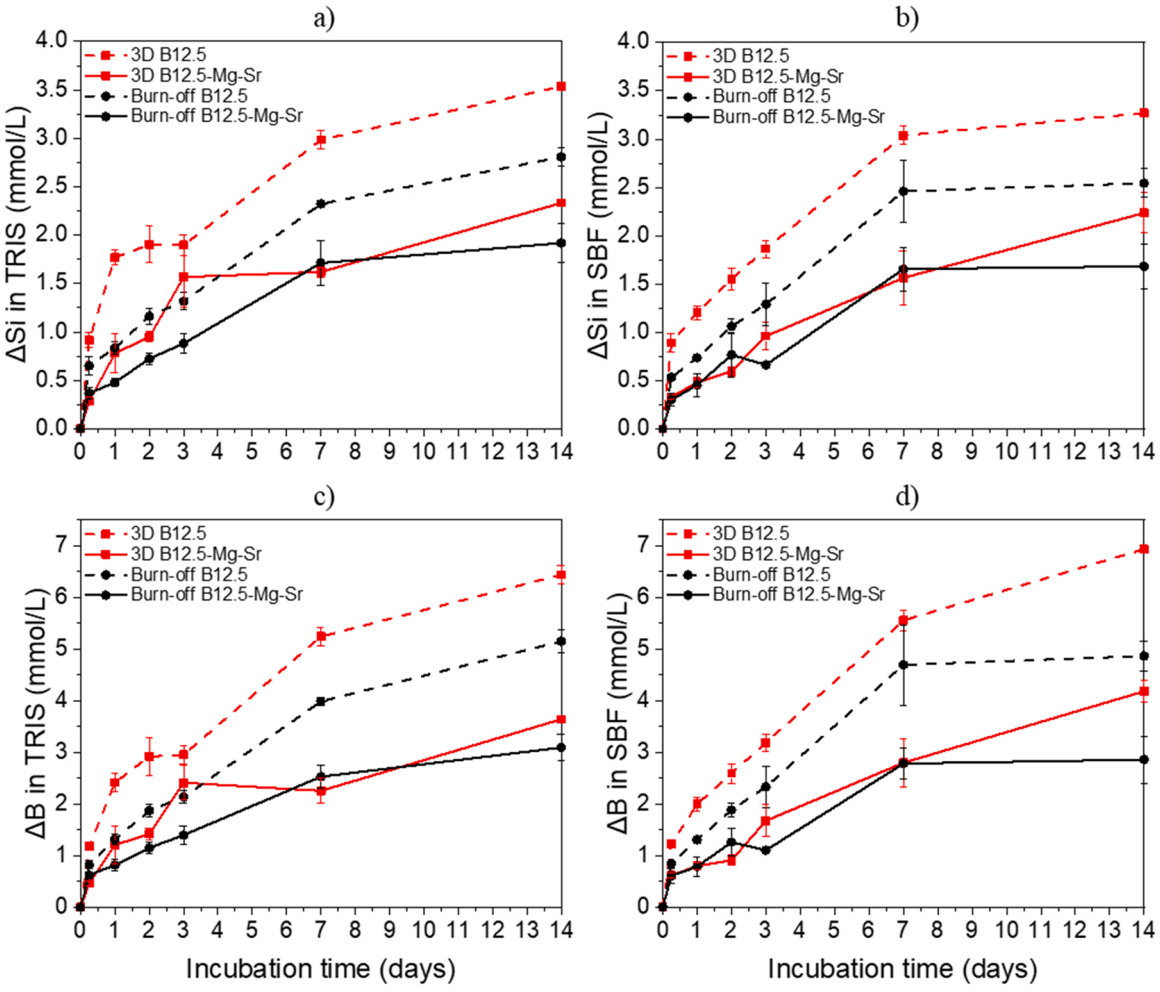

Fig. 5. Concentrations of a-b) Si and c-d) B after static in vitro dissolution in TRIS and SBF for up to 14 days. ΔElement = [Element] in TRIS/SBF in the presence of the sample – [Element] in TRIS/SBF initial solution.

inside the construct [4].

The sizes of pores in the 3D printing scaffolds are reported in the Table 4 and are all above the 100 μm required for the migration of MC3T3-E1 and mesenchymal stem cells, which have sizes between 20 and 50 μm and 13–30 μm, respectively. [40,41]. The pore sizes of scaffolds produced by porogen burn-off are quite inhomogeneous, ranging from micropores to pores of few millimeters.

Overall, scaffolds made from B12.5 and B12.5-Mg-Sr glass compositions meet the porosity and pore size required in bone tissue engineering. 3D printed scaffolds offer better pore size homogeneity when compared to those obtained by porogen burn-off. Moreover, interconnective porosity, as found in the 3D printed scaffolds, is known to permit cell migration inside of the scaffolds, diffusion of nutrients and removal of waste from the scaffold [42].

3.1.2. *Mechanical properties*

The mechanical properties of the implant should mimic the mechanical properties of the natural tissue. The compressive strengths of B12.5 scaffolds produced by the burn-off method and 3D printing were 1.5 ± 0.2 and 2.5 ± 0.7 MPa, respectively, as seen in the Fig. 3. Significantly higher values were obtained with B12.5-Mg-Sr composition, 8.9 ± 2.4 and 6.1 ± 1.8 MPa for scaffolds produced by burn-off and 3D printing, respectively. Addition of Mg to the glass composition lowers the glass viscosity which, consequently, improves the sintering properties and improves scaffolds strength [43,44]. Addition of Sr widen the sintering temperature window, which allows sintering at higher temperature above Tg. Moreover, the strength is greatly affected by the porosity. Thus, the increase in strength can also be linked to the lower porosities of B12.5-Mg-Sr scaffolds, as seen in Table 3 [9]. Summarizing, the strengths of sintered glass scaffolds were mostly within the 2–12 MPa strength of trabecular bone [45]. It has been reported that hip stems are subjected to 3–11 MPa loading and tibial bones to approximately 4 MPa stresses [46,47].

3.1.3. *Static in vitro dissolution in TRIS and SBF*

To study the effect of static in vitro dissolution and bioactivity, scaffolds were incubated in TRIS and SBF solution for up to 14 days. In vitro dissolution tests performed in TRIS aimed to assess the ions released from the glass during dissolution. In SBF, the ability of the released ions to saturate the solution, thus leading to the precipitation of HA, is being studied. Change in pH, mass loss and ion concentrations were investigated.

Fig. 2 presents the pH of TRIS and SBF solutions as a function of the incubation time for both glass compositions, manufactured into 3D printed and burn-off scaffolds. For all scaffold types and compositions, there is a rise in pH with increasing immersion time followed by stabilization around the 7th day (Fig. 4a-b). The initial increase in pH is related to the ion release of silicate and borosilicate glasses, as already shown in previous studies [14,15]. The stabilization in pH can be attributed to the solution becoming saturated with ions and subsequent formation of the HA layer [48]. The pH profile is similar in both TRIS and SBF. Immersion of B12.5 glass composition results in higher pH

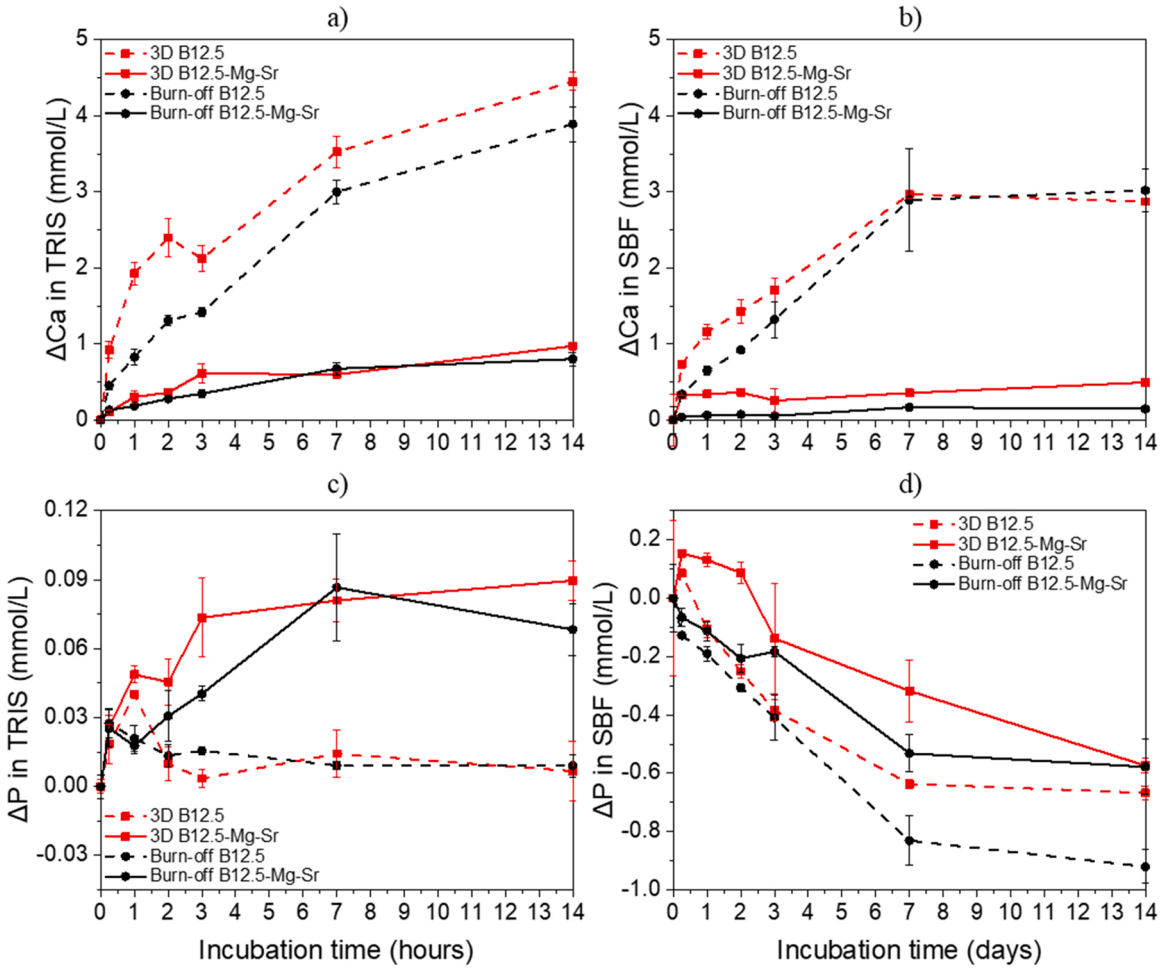

Fig. 6. Concentrations of a-b) Ca and c-d) P after static in vitro dissolution in TRIS and SBF for up to 14 days. ΔElement = [Element] in TRIS/SBF in the presence of the sample – [Element] in TRIS/SBF initial solution.

compared to B12.5-Mg-Sr in both solutions. The rise of pH is also more significant in 3D printed scaffolds than in burn-off scaffolds. The pH of the solution in all groups of scaffolds can increase to, or even exceed, pH= 8 after 7 days. This indicates that the scaffold dissolution is rapid and, if not carefully controlled, may be toxic for cells [49]. These results are also indicative of a faster dissolution of B12.5 scaffolds, resulting in rise of ions and consequently higher pH levels. B12.5-Mg-Sr scaffolds dissolve slower due to the stabilizing effect of Mg and Sr on glass network [15,16]. Substitution of SrO and MgO for CaO results in increase in BO_3 at the expense of BO_4 units [14]. Consequently, changing the ratio between bridging and non-bridging oxygen leading to stabilization of the borate network.

When compared, despite their overall porosity being similar (Tables 2), 3D printed scaffolds produce higher pH levels than burn-off scaffolds. It can be explained by a more interconnected porosity for the 3D printed scaffolds resulting in higher surface area in contact with the immersion solution.

Fig. 4c-d presents the mass loss (Eq.2) as a function of the incubation time for both glass compositions manufactured into 3D printed and burn-off scaffolds. The mass loss is observed for all scaffolds indicating that degradation occurred. Mass loss is significantly higher for B12.5 than for B12.5-Mg-Sr scaffolds. This agrees with in vitro dissolution test performed by Tainio et al., showing that substitution of CaO with SrO and/or MgO have stabilizing effect on borate network and help to decrease the dissolution rate [14]. Results also implies that the impact of composition is dominant over the scaffold preparation techniques. Moreover, 3D printed scaffolds tend to have larger mass loss compared to burn-off scaffolds. This is also in accordance with pH data and is most probably related to the higher surface area of the 3D printed scaffolds. The ion concentrations in TRIS and SBF after static in vitro dissolution were analyzed using ICP-OES. Si and B are backbone of the glass network and thus their release profiles inform about the glass dissolution trend. The release profiles of B and Si are quite identical in both SBF and TRIS solutions (Fig. 5).

For all scaffold types and compositions, there is a linear increase in Si^{4+} and B^{3+} ion release until 7th day after which it stabilizes significantly. Highest Si^{4+} and B^{3+} ion release is observed from B12.5 glass scaffolds. Moreover, the ion release is higher from 3D printed scaffolds compared to the burn-off scaffolds. These observations are in agreement with pH results and further confirm faster dissolution of B12.5 glass composition as well as faster dissolution of the 3D printed scaffolds.

The Ca and P release profiles (Fig. 6) are important as they give information about precipitation of HA-like layer, which is often seen as a first sign of bioactivity [50]. The release profile of Ca in TRIS and SBF is characterized by linear increase until 7th day, after which the release slows down (Fig. 6a-b).

Ca release in both TRIS and SBF is higher from B12.5 compared to B12.5-Mg-Sr scaffolds. It could be caused by significantly more Ca in B12.5 glass network. Moreover, the Ca release is highest for 3D printed scaffolds compared to the burn-off scaffolds. Although, this difference was not always significant.

In TRIS, the P^{3-} ion concentrations remains stable for the B12.5 scaffolds (Fig. 6c). However, it rises with increasing immersion time for the B12.5-Mg-Sr scaffolds. These results can be explained by

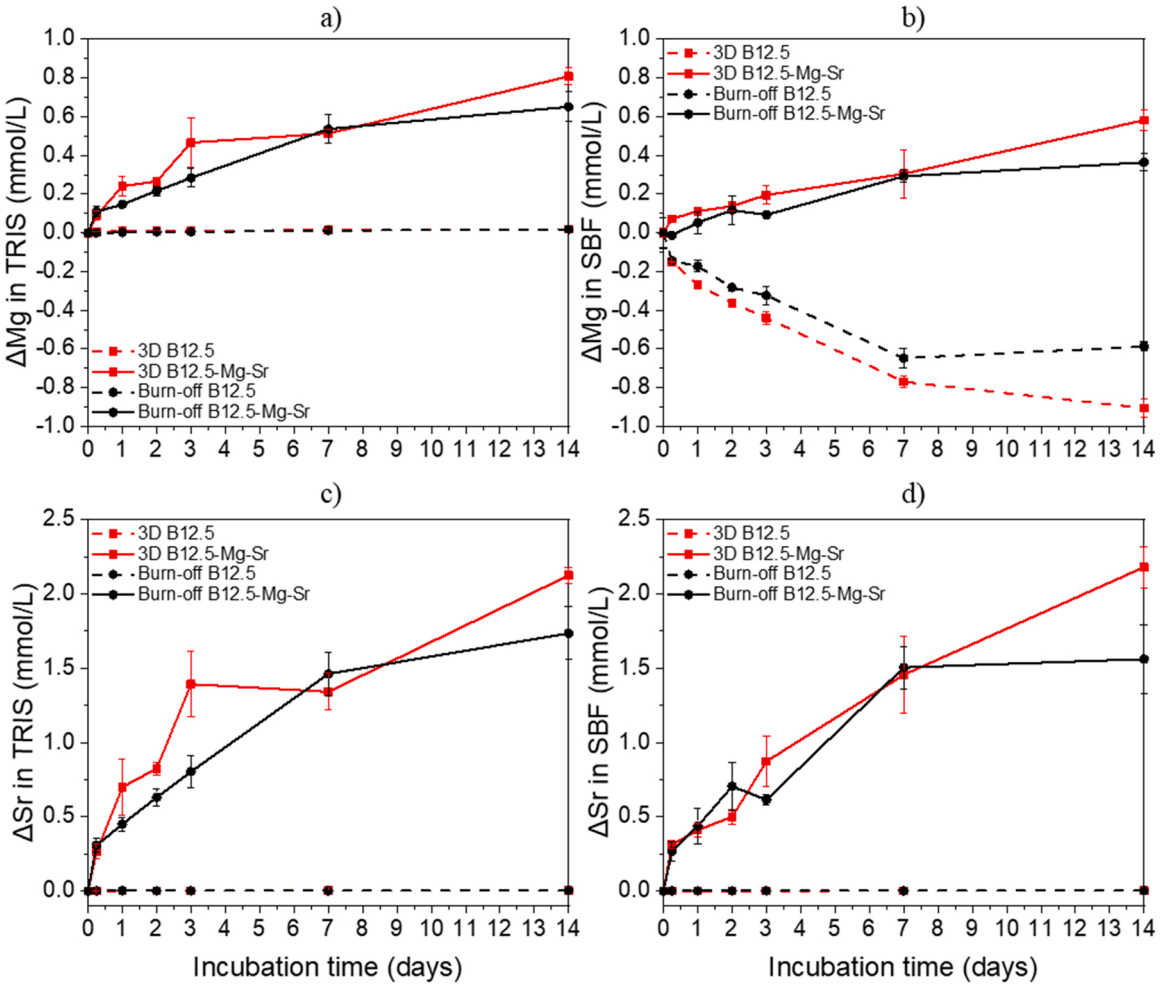

Fig. 7. Concentrations of a-b) Mg and c-d) Sr after static in vitro dissolution in TRIS and SBF for up to 14 days. ΔElement = [Element] in TRIS/SBF in the presence of the sample – [Element] in TRIS/SBF initial solution.

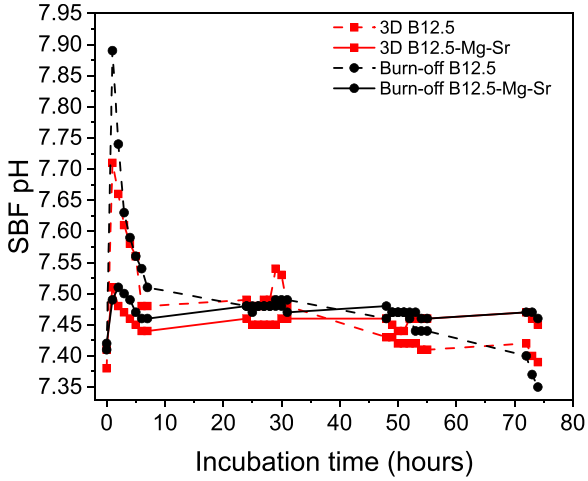

Fig. 8. pH of SBF after dynamic in vitro dissolution for up to 74 h.

simultaneous release and precipitation of phosphorus. Differences in P^{3-} ion release between 3D printed scaffolds and burn-off scaffolds in TRIS are not significant.

In SBF, simultaneous dissolution and precipitation of P, results in overall P consumption (Fig. 6d). This consumption reaches a plateau after day 7th. Moreover, P release for B12.5 groups were significantly lower. This can be linked to a slower HA precipitation when Ca is replaced with Mg and/or Sr containing silicate bioactive glasses as discussed in [15,16]. Finally, the P consumption, from the SBF, appears to be faster for the scaffolds produced by burn-off scaffolds. This consumption of P indicates precipitation of Ca-P layer, which is an indication of the scaffolds' bioactivity [50].

B12.5 glass composition does not contain MgO so as expected Mg was only released from B12.5-Mg-Sr glass composition in TRIS (Fig. 7a). In SBF, Mg concentration decreases significantly for B12.5 glass composition and raises slowly for B12.5-Mg-Sr composition over the course of the immersion in SBF (Fig. 7b). Burn-off scaffolds releases slightly less Mg^{2+} ions than 3D printed scaffolds in TRIS. However, in SBF the Mg concentration is smaller for 3D printed scaffolds. The slow release, and the decrease in some cases, of Mg concentration could be indicative that part of the Mg is consumed and incorporated into the reactive layer [16].

Finally, as expected from the glass composition, the Sr concentration remains null in the solution containing the B12.5 glass, whereas it rises with increasing immersion time for the scaffolds made from the B12.5-Mg-Sr glass composition (Fig. 7c-d). Burn-off scaffolds releases slightly more ions compared to 3D printed scaffolds. From past research, it is highly probable that part of the strontium is also incorporated in the reactive layer [15].

Summarizing, ICP results are in agreement with pH results and further confirm faster dissolution of B12.5 glass composition as well as faster dissolution of 3D printed scaffolds. This results are in accordance with previous reports, where slower dissolution rate and HA

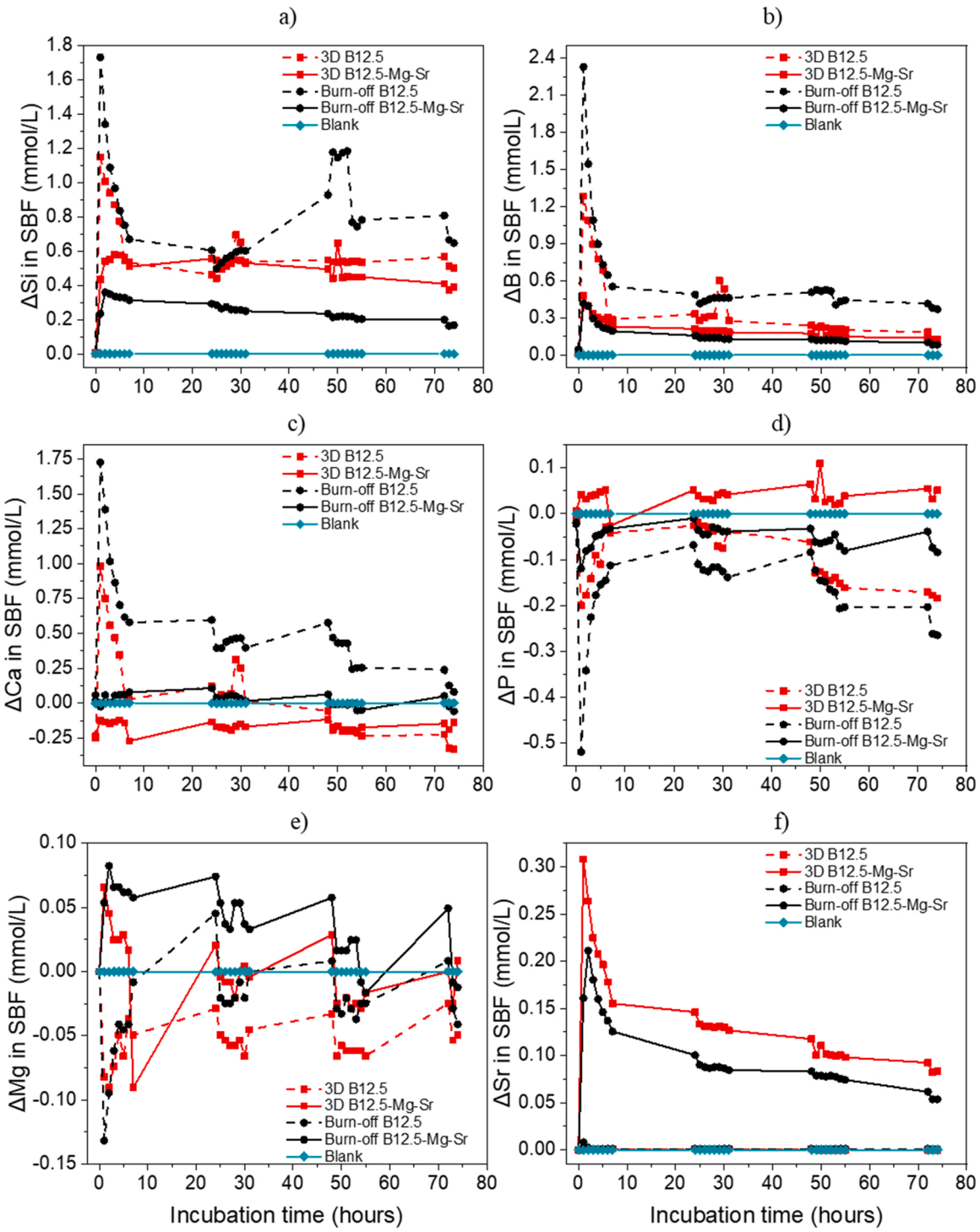

Fig. 9. Concentrations of a-f) Si, B, Ca, P, Mg and Sr in SBF after dynamic in vitro dissolution test with scaffolds for up to 74 h. ΔElement = [Element] in SBF in the presence of the sample – [Element] in SBF initial solution.

precipitation was observed with Mg and Sr containing silicate bioactive glasses [15,16].

Moreover, bioactivity of all scaffolds is indicated by HA precipitation, which is faster for B12.5 than for B12.5-Mg-Sr scaffolds. Finally, based on release profiles it seems that ions releases stabilize after 7th day. These results also agree with previous studies done with B12.5 and B12.5-Mg-Sr glass compositions [14].

3.1.4. *Dynamic in vitro dissolution in in SBF*

To investigate the effect of dynamic in vitro dissolution on scaffolds degradation and bioactivity, scaffolds were incubated in SBF solution for up to 72 h. Change in pH and ion concentrations were investigated. Fig. 8 presents the pH change in SBF as a function of the incubation time for both glass compositions, B12.5 and B12.5-Mg-Sr, manufactured into 3D printed and burn-off scaffolds. For all scaffolds, there is a drastic increase in pH after the first hour for all scaffolds and then the pH goes rapidly down and stabilizes after 7 h. The increase in pH is more pronounced for the B12.5 glass composition. No significant difference is seen between the B12.5-Mg-Sr scaffolds produced by either of the utilized techniques. The pH values in the dynamic conditions remain stable

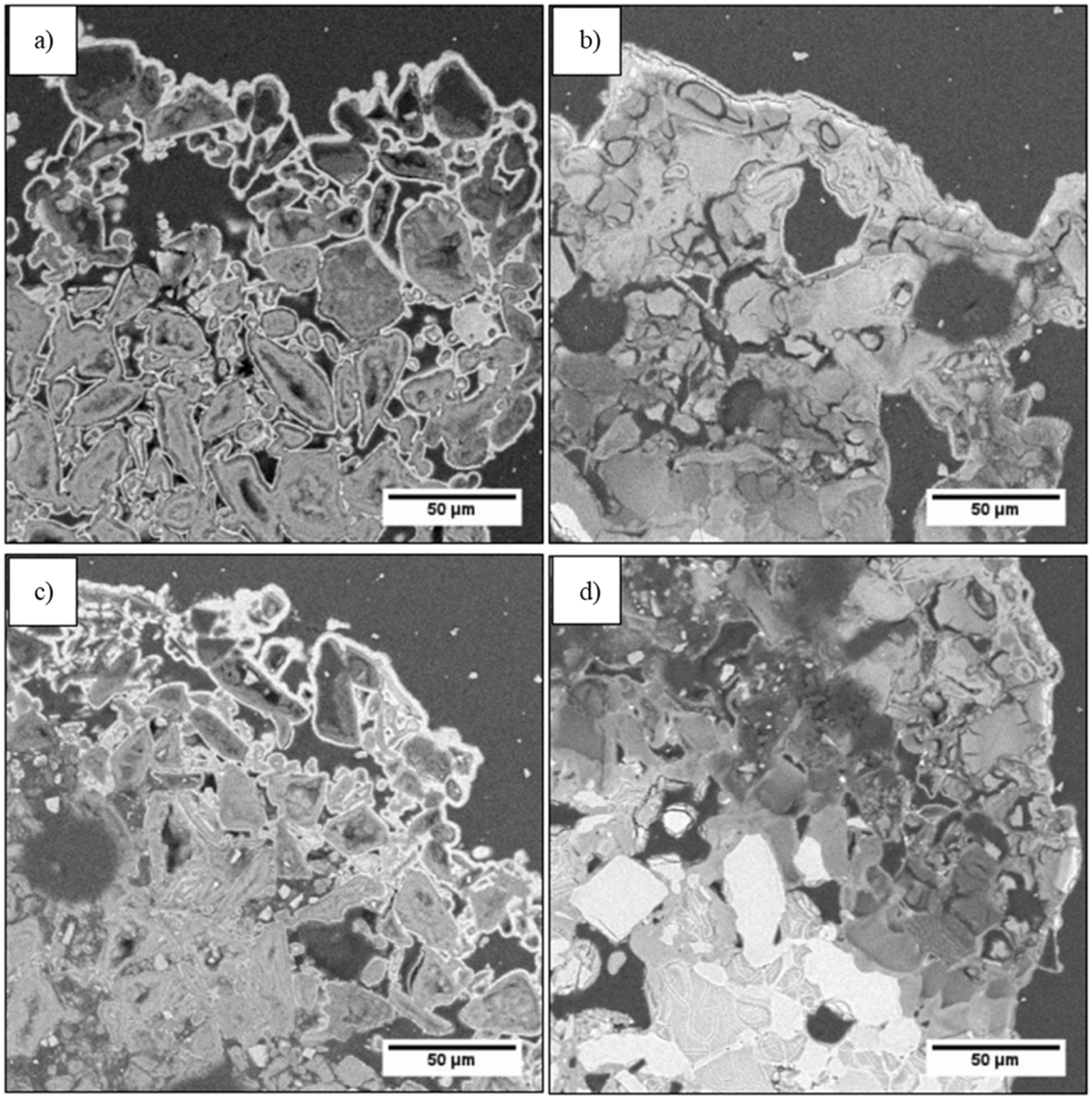

Fig. 10. SEM images of scaffolds after 336 h of immersion in SBF at 250x magnifications. SEM images of (a,c) B12.5 and (b,d) B12.5-Mg-Sr scaffolds produced via (a, b) burn-off and (c,d) 3D printing methods.

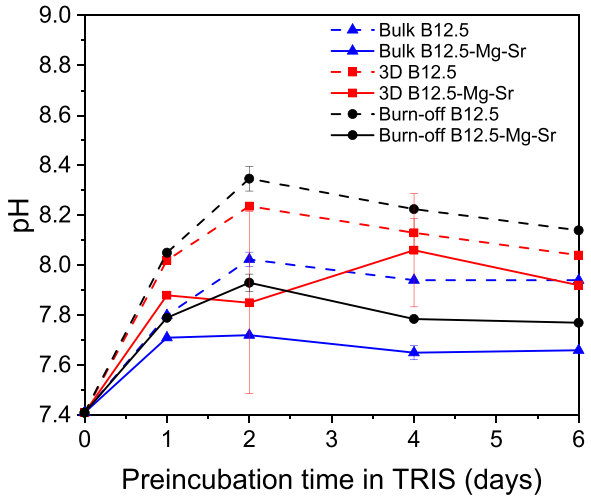

Fig. 11. pH of TRIS after preincubation with scaffolds for up to 6 days.

in the range of 7.4–7.5 for all the scaffolds. Only a burst of ions is seen within the first 6 h. These pH values are appropriate for the culture of cells.

The ion concentrations in SBF after dynamic in vitro dissolution were analyzed using ICP-OES (Fig. 9). The release profiles of Si and B scaffolds are characterized by initial burst of ions reaching its peak after 1 h. Ion concentrations decrease and stabilize after 7 h (Fig. 9a-b). This dissolution behavior is characteristic of dynamic condition and has been reported before [51]. The burst ion release is more significant for B12.5 scaffolds compared to B12.5-Mg-Sr scaffolds. Highest Si^{4+} ion release from B12.5 is observed from burn-off scaffolds, and with B12.5-Mg-Sr scaffolds from 3D printed scaffolds, respectively.

With B12.5-Mg-Sr composition, no significant difference between dissolution of the burn-off and 3D printed scaffolds is observed. The increased pH and Si release for the burn-off scaffold is unexpected based on the higher surface area of the 3D printed scaffolds. However, such discrepancy can be due to the ability of the liquid to flow through the various samples [29]. Indeed, the smaller pore size and lower interconnectivity between pores in the burn-off scaffolds could also lead to longer liquid reminiscence time in contact with the sample, thus leading

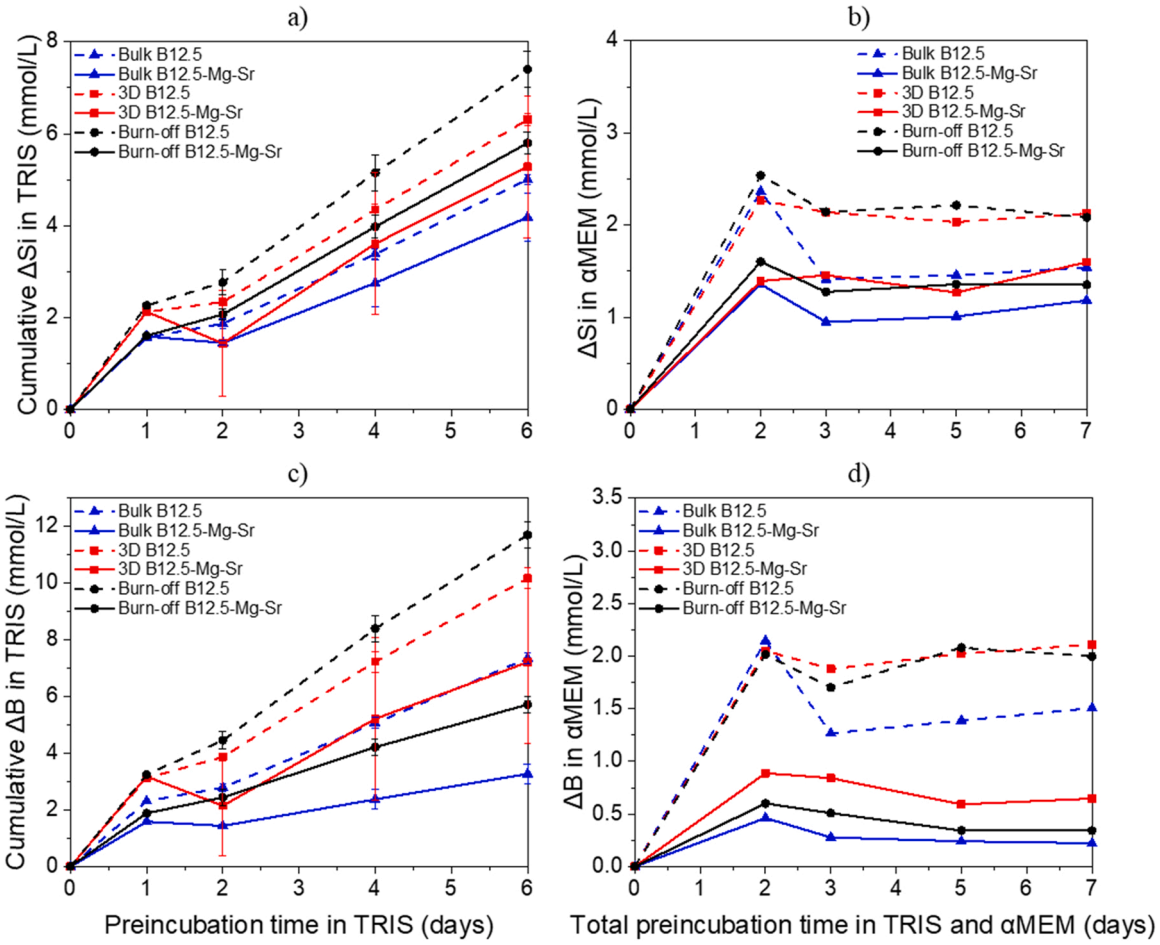

Fig. 12. Concentrations of a-b) Si and c-d) B in TRIS and αMEM culture medium after preincubation with scaffolds for up to 7 days. ΔElement = [Element] in TRIS/ αMEM in the presence of the sample – [Element] in TRIS/ αMEM initial solution.

to more extended degradation. This is of particular interest and to keep in mind in future investigation of scaffolds in a dynamic context.

Ca^{2+} ion concentration levels are highest for B12.5, and P^{3-} ion concentrations are highest for B12.5-Mg-Sr scaffolds (Fig. 9c-d). Ion release profiles of Ca^{2+} from B12.5 scaffolds are characterized by initial burst of ions during the first hour of immersion, followed by strong decrease and stabilization after 7 h. For B12.5-Mg-Sr glass, Ca^{2+} ion release profiles are mostly stable from the beginning of the immersion. Ion release profiles of P^{3-} is characterized by initial consumption of ions during first hours of immersion, followed by increase and stabilization after 7 h. Burn-off scaffolds produce higher Ca^{2+} ion concentration levels than 3D printed scaffolds. However, 3D printed scaffolds produce higher P^{3-} ion concertation levels than burn-off scaffolds.

As expected, Mg^{2+} and Sr^{2+} ion release is highest for B12.5-Mg-Sr scaffolds, since B12.5 glass composition does not contain these elements. Mg release (Fig. 9e) was not found to be stable, which could be explain by simultaneous release and precipitation of Ca-P reactive layer that can also include Mg [16]. Sr release profile is characterized by initial burst of ions, followed by strong decrease after 1 h and stabilization after 7 h (Fig. 9f). most likely due to the incorporation of Sr into the reactive layer. Moreover, 3D printed scaffolds release more Sr^{2+} ions that burn-off scaffolds.

Generally, ion concentrations are notably lower during dynamic in vitro dissolution compared (Fig. 9) to static in vitro dissolution (Figs. 5–7). This is in accordance with previous research reporting that dynamic conditions can help to avoid a rapid and drastic fluctuation of pH [51,49,52]. The initial burst release of ions is significantly higher for B12.5 compared to B12.5-Mg-Sr glass composition. After burst release, ion releases stabilize and are lower than in static condition. Moreover, dynamic conditions resemble human body environment more accurately than the static ones, as in physiological conditions fluids are constantly washed away [49]. In this respect, dynamic conditions could be more optimal for in vitro cell growth. Finally, consumption of Ca and P from immersion solution indicate, as seen in Fig. 6, that formation of most likely HA layer takes place.

3.1.5. SEM

SEM imaging was used to analyze scaffolds after 336 h of static immersion in SBF. The sintered scaffolds had high levels of internal microporosity (Fig. 10a, c) showing loose particles suggesting insufficient sintering of B12.5. Moreover, internal microporosity of B12.5-Mg5-Sr10 scaffolds seems to be more compact indicating Mg and Sr ability to promote sintering.

In all SEM images a bright layer appears at the surface of the grains exposed to the solution. This bright layer was found to be rich in calcium and phosphorus and was earlier found to be assigned to the precipitation of a reactive layer [9]. Elemental compositions of unreacted glass and formed surface layers for scaffolds produced via porogen burn-off and robocasting were analyzed and are presented in Table S3.

Furthermore, the FTIR spectra of the glass scaffolds pre and post-immersion were recorded and are reported in Figure S4. FTIR spectra confirm the precipitation of a reactive layer. The change in the molecular vibration is indicative of the typical dissolution of the glass network and precipitation of reactive layer within the HA domain.

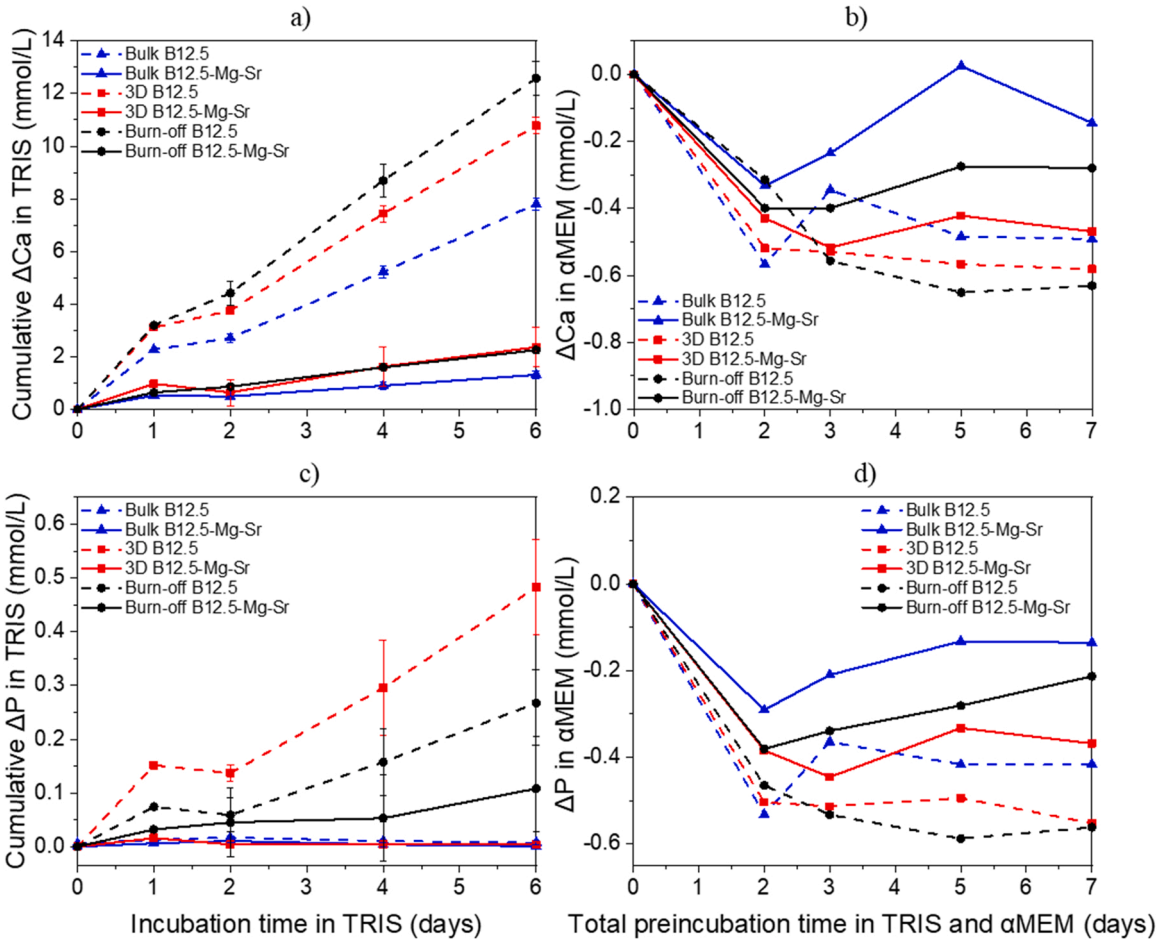

Fig. 13. Concentrations of a-b) Ca and c-d) P in TRIS and αMEM culture medium after preincubation with scaffolds for up to 7 days. ΔElement = [Element] in TRIS/ αMEM in the presence of the sample – [Element] in TRIS/ αMEM initial solution.

3.2. Cell analysis

3.2.1. Effect of preincubation on ion release

To investigate the effect of preincubation on ions release profiles, scaffolds were preincubated for up to 6 days in TRIS, following additional 24 h in αMEM. The pH levels of TRIS during preincubation are presented in Fig. 11.

There is an increase in pH for all scaffolds until 2 days except for bulk and 3D printed B12.5-Mg-Sr, where the increase stopped at 1 day. This indicates that the scaffold dissolution in TRIS is rapid. Then, the pH slightly decreased and stabilized. The pH peak of TRIS solution with the scaffolds is reached at pH≥ 8 for B12.5 and pH≥ 7.7 for B12.5-Mg-Sr scaffolds. Slower increase of pH with B12.5-Mg-Sr glass composition can be explained by stabilizing effect of Mg and Sr consequently, resulting in a slower dissolution rate of B12.5-Mg-Sr scaffolds and thus smaller pH levels.

For B12.5 glass composition, the pH rise was most pronounced for the burn-off scaffolds. For B12.5-Mg-Sr composition the pH rise was most pronounced for 3D printed scaffold. For both glass compositions, bulk scaffolds produced lower pH rise compared to other scaffold types. The difference between bulk, burn-off and 3D printed scaffolds could be explained by their different porosities (Table 3&4). Dissolution of scaffolds with higher porosity and consequently surface area, result in higher ion and pH levels and thus, dissolution of more porous and more reactive B12.5 scaffolds can result in higher pH levels compared to less porous/reactive B12.5-Mg-Sr scaffolds. Furthermore, 3D printed and burn-off scaffolds with higher porosity compared to bulk scaffolds also produced higher pH levels during dissolution. The ion concentrations in TRIS and αMEM after preincubation test were analyzed using ICP-OES (Fig. 12). The ICP results for Si and B were in accordance with measured pH levels; ion concentrations expressed higher for B12.5 than for B12.5-Mg-Sr scaffolds in TRIS and αMEM.

The release profiles of Si and B in TRIS were increasing linearly (Fig. 12a, c). Highest Si^{4+} and B^{3+} ion concentrations in TRIS were observed for B12.5 burn-off scaffolds, and lowest for B12.5-Mg-Sr bulk scaffolds.

In αMEM, the highest ion concentrations were observed for burn-off and 3D printed B12.5 scaffolds, and lowest for B12.5-Mg-Sr bulk scaffolds (Fig. 12b, d). Most importantly, after 2nd day of total preincubation time, Si^{4+} and B^{3+} ion concentrations in αMEM decrease and stabilize at day 3.

Ca^{2+} ion concentrations were highest for B12.5 composition when compared with B12.5-Mg-Sr scaffolds in TRIS, but lowest in αMEM (Fig. 13a-b).

P^{3-} ion concentrations were highest for B12.5-Mg-Sr scaffolds compared with B12.5 scaffolds in both TRIS and αMEM (Fig. 13c-d). The release profiles of Ca and P in TRIS increased linearly (Fig. 13a-c). Most importantly, after 48 h of total preincubation time, Ca^{2+} and P^{3-} ion concentrations in αMEM decrease and stabilize at day 3 (Fig. 13b-d). Moreover, highest Ca^{2+} and P^{3-} ion concentrations in TRIS and αMEM are observed for burn-off and bulk scaffolds, respectively.

Consumption of Ca and P in αMEM, indicate that precipitation of Ca-P rich layer precipitate already after 2 days of total preincubation time. The precipitation was faster for B12.5 scaffolds due to their faster dissolution [14] and consequently faster oversaturation of αMEM with ions.

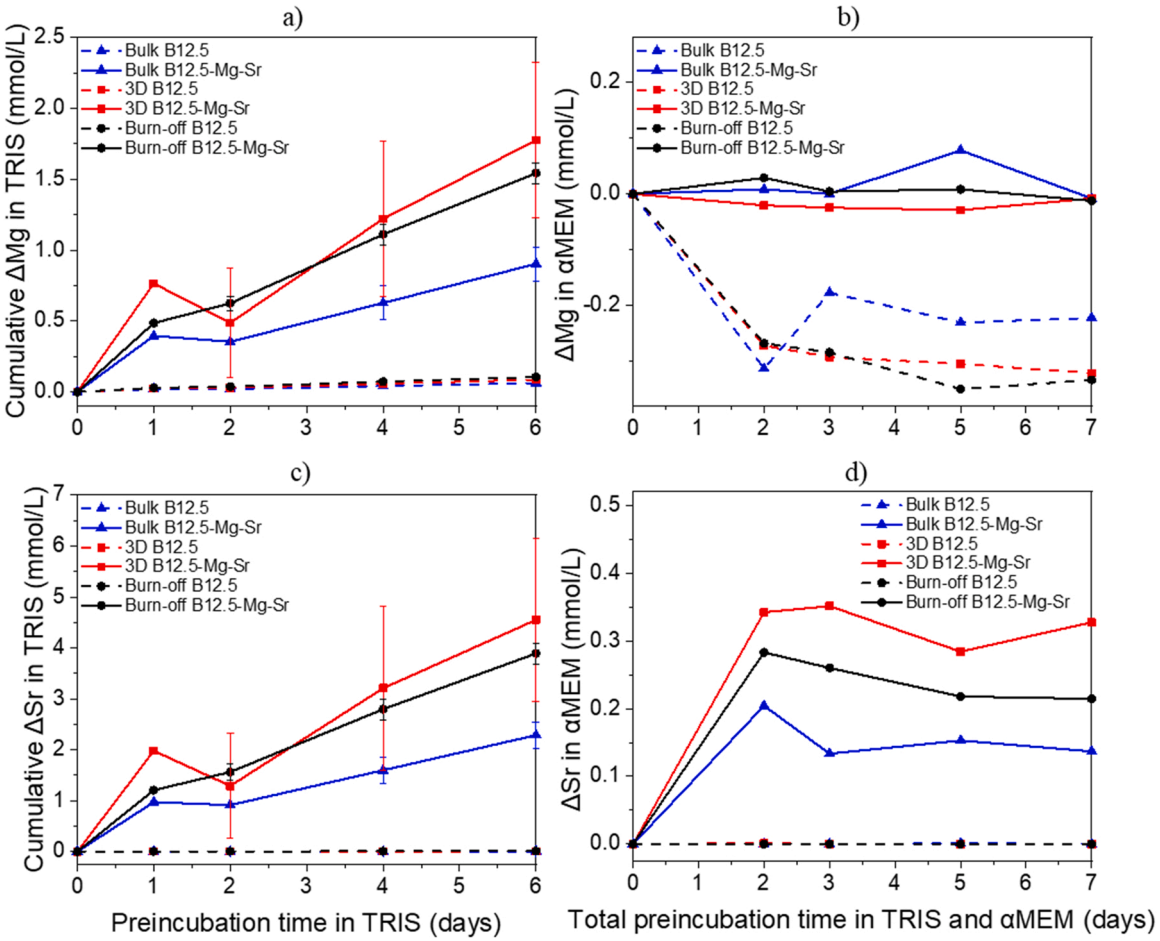

Fig. 14. Concentrations of a-b) Mg and c-d) Sr in TRIS and αMEM culture medium after preincubation with scaffolds for up to 7 days. ΔElement = [Element] in TRIS/ αMEM in the presence of the sample – [Element] in TRIS/ αMEM initial solution.

Mg^{2+} and Sr^{2+} ion concentrations, as expected from glass compositions, were highest for B12.5-Mg-Sr composition in both preincubation solutions. B12.5 scaffolds do not produce any Mg^{2+} and Sr^{2+} ion release (Fig. 14). Only in αMEM consumption of Mg from B12.5 scaffolds is observed (Fig. 14b). This consumption could be related to precipitation of reactive layer with incorporated Mg.

Mg^{2+} and Sr^{2+} ion release from B12.5-Mg-Sr scaffolds in TRIS were increasing linearly (Fig. 14a, c). In αMEM, Mg and Sr^{2+} ion release stabilized after 2 days of total preincubation (Fig. 14b, d). Highest Mg^{2+} and Sr^{2+} ion release in TRIS was observed for 3D printed scaffolds. In αMEM, highest Mg^{2+} and Sr^{2+} ion release was observed from bulk and 3D printed scaffolds, respectively.

In conclusion, ICP results tend to indicate that after 2 days of preincubation (1 day in TRIS and 1 day in αMEM) still exhibit significant ion release. At 3 days of total preincubation (2 days in TRIS and 1 day in αMEM) the ion release exhibits a plateau most likely related to the precipitation of hydroxyapatite. Therefore, it was concluded that 3 days of total preincubation is optimal to control the excess ion release. This is in accordance with literature review by Ciraldo et al., in which it was suggested that highly porous BAG scaffolds, with more than 21 wt% of Na_2O should be preincubated for more than 72 h before static cell culture [49].

3.2.2. *Effect of glass composition on cell survival and ion release*

MC3T3-E1 cells were used for initial evaluation of the impact of the glass composition on cell survival. For this experiment, bulk scaffolds were preincubated for 2 or 7 days in TRIS always followed by 24 h in αMEM.

Fig. 15 shows MC3T3-E1 cell viability images after 24 h of culture with B12.5 and B12.5-Mg-Sr bulk scaffolds. These scaffolds were preincubated two or seven days before culture. There were significantly more live cells in the bottom of wells with B12.5-Mg-Sr scaffolds compared to B12.5 after the pre-incubations (Fig. 15a-d). In fact, cell survival around B12.5-Mg-Sr glass scaffolds is comparable to cell survival in the control. Cell survival at the top of the scaffolds (Fig. 15A-D), was better with B12.5-Mg-Sr glass composition. Longer preincubation slightly improved cell survival with B12.5 glass composition. The effect of longer preincubation time on cell survival at the top of B12.5-Mg-Sr scaffolds did not seem significant.

Better cell survival with B12.5-Mg-Sr scaffolds could be due to stabilizing properties of Mg and Sr. It is expected that, less stabilized B12.5 glass dissolves faster, causing a rise in pH to levels that would be toxic for the cells. This ion release can be further decreased by longer preincubation of 7 days in TRIS.

Longer preincubation led to a better cell survival with B12.5 scaffolds but still not comparable to the control. Moreover, even after longer preincubation, B12.5-Mg-Sr glass still seemed less toxic for the cells than B12.5. The effect of preincubation time was not significant for B12.5-Mg-Sr glass composition, because shorter preincubation already prevented toxic ion burst released while maintaining an ion release of interest.

Cell survival at the top of the bulk scaffolds (Fig. 15A-D), is better with B12.5-Mg-Sr glass composition. Longer preincubation slightly improve cell survival with B12.5 glass composition. The effect of longer preincubation time on cell survival at the top of B12.5-Mg-Sr scaffolds is not significant.

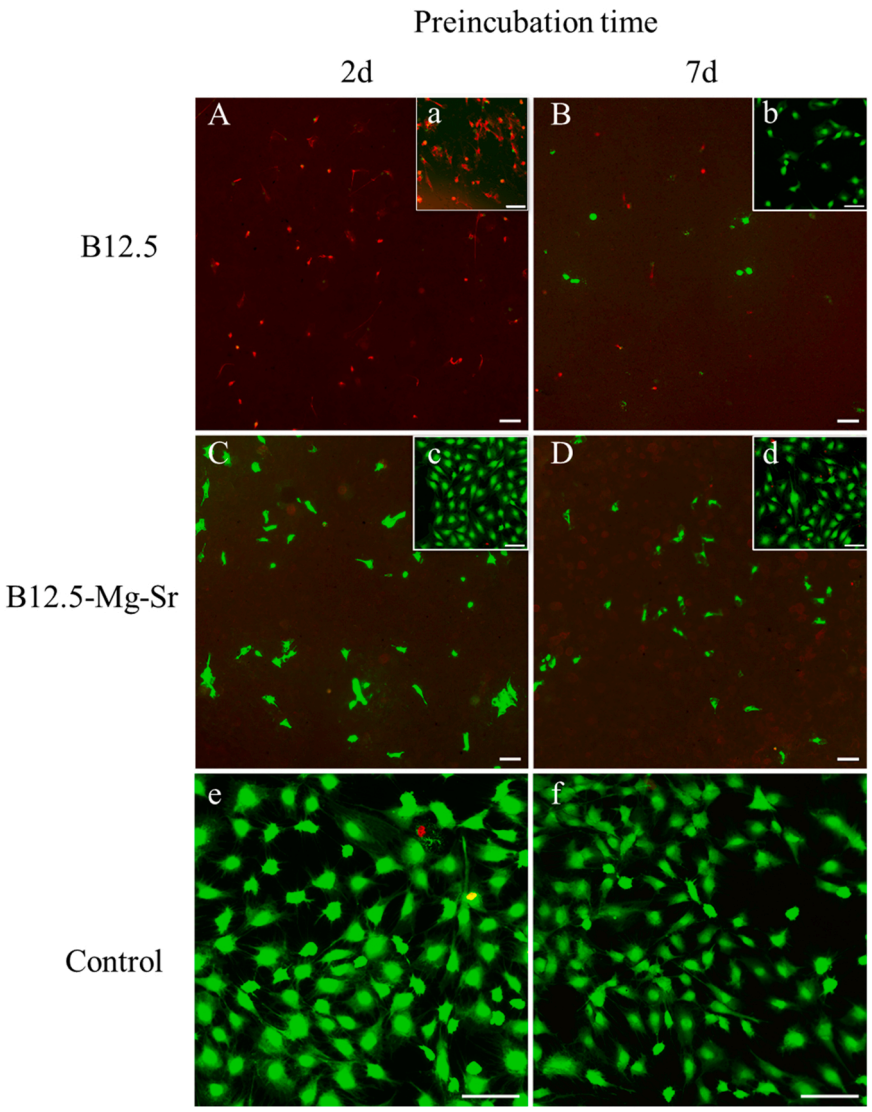

Fig. 15. Fluorescent images of MC3T3-E1 cells after 24 h of culture in αMEM culture medium. Images A-D show the top of the bulk scaffolds. Images a-f show the bottom of the wellplate. Viable (green) and necrotic (red) cells were stained with Calcein AM and Ethidium homodimer-1 respectively. Scale bar 100 μm.

The ion concentrations in αMEM after culture with cells were analyzed using ICP-OES (Fig. 16). Si^{4+} ion concentrations increased for both glass compositions and were higher than in the cell culture media (positive control; cells growing without scaffold presence). Longer preincubation time of 7 days resulted in smaller ion concentrations for both glass compositions.

However, this decrease is significant only for B12.5 scaffolds. In scaffolds preincubated for 2 days, B12.5-Mg-Sr glass composition produced slightly smaller Si^{4+} ion release. There is no difference between ion release from scaffolds preincubated for 7 days.

B^{3+} ion concentrations increased for both glass compositions and were significantly higher than in control cell culture media, which does not initially contain boron. Most importantly, even after both preincubation times, B12.5 scaffolds produce significantly larger B^{3+} ion release, whereas longer preincubation time of 7 days resulted in significant decrease in B^{3+} ion concentrations for B12.5 scaffolds. For B12.5-Mg-Sr scaffolds, no difference in ion release between different preincubation times were observed. It has been reported that B concentrations above 0.65 mmol were shown to decrease the growth and proliferation rate of bone marrow cells (BMSc) [53]. Similar results were reported by Brown et al. where B concentrations of 1.5 mmol in the culture medium inhibits cell proliferation [11]. In our study, the non-cumulative B concentration for B12.5 scaffolds were around 26 and 17 after 2 and 7 days of total preincubation time, respectively. The non-cumulative B concentration for B12.5-Mg-Sr bulk scaffolds were around 3.2 and 2.4 after 2 and 7 days of total preincubation time, respectively. This could explain why B12.5 scaffolds were more cytotoxic compared to B12.5-Mg-Sr scaffolds.

Ca^{2+} ion concentrations decreased with both glass composition scaffolds, and concentrations were smaller than in control cell culture media. Notably, for both preincubation times, B12.5 scaffolds produce significantly smaller Ca^{2+} ion concentrations. Longer preincubation time of 7 days results in larger ion concentrations for B12.5 scaffolds. Different preincubation times have no significant impact of Ca^{2+} ion release from B12.5-Mg-Sr scaffolds.

P^{3-} ion concentrations can be seen to decrease for B12.5-Mg-Sr and increase B12.5 scaffolds, respectively. Longer preincubation time of 7 days resulted in decrease of P^{3-} ion release from B12.5 scaffolds, while different preincubation times had no significant impact of P^{3-} ion release from B12.5-Mg-Sr scaffolds.

ICP results indicate that Ca consumption is faster with cell cultures in the presence of B12.5 scaffolds. Most probably, due to higher dissolution rate of B12.5, culture medium could be oversaturated with Ca faster, leading to faster precipitation of CaP compared to B12.5-Mg-Sr

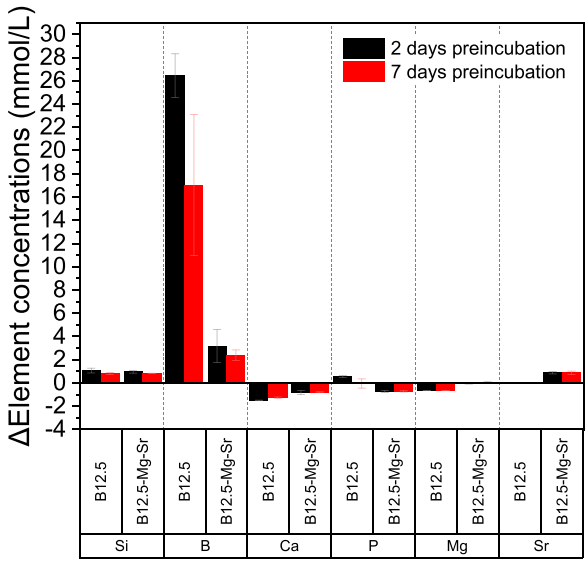

Fig. 16. Concentrations of Si, B, Ca, P, Mg and Sr in αMEM culture medium after culturing Bulk B12.5 and B12.5-Mg-Sr scaffolds for 24 h with the MC3T3-E1 cells as a function of time. ΔElement = [Element] in αMEM in the presence of the sample – [Element] in αMEM initial solution.

scaffolds. Moreover, content of Ca in B12.5 is significantly larger than in B12.5-Mg-Sr glass composition. However, P seems to be consumed slower with B12.5 than B12.5-Mg-Sr scaffolds. This could be due to P release from B12.5 being significantly larger than simultaneous P precipitation.

Since there is no Mg and Sr in B12.5 glass composition, their release is observed only for B12.5-Mg-Sr glass composition. With B12.5 scaffolds, Mg content decreases after 24 h of cell culture and Sr release stays at positive control level. This could be explained by precipitation of Mg from culture medium together with Ca-P layer. Longer preincubation time of B12.5-Mg-Sr and B12.5 scaffolds does not result in any significant change compared to shorter preincubation time.

In the study by Gentlemen et al. Sr concentrations between 5 and 23 ppm resulted in Saos-2 osteoblast cells activity and inhibited osteoclasts differentiation [54]. In our study, non-cumulative Sr release from 12.5-Mg-Sr scaffolds, after 2 and 7 days of total preincubation time, were significantly higher, around 78 ppm. Despite, that MC3T3-E1 cells shown better viability and survival with B12.5-Mg-Sr compared to B12.5 bulk scaffolds, which can indicate that levels of Sr around 78 ppm are not cytotoxic.

Overall, ion release from B12.5 and B12.5-Mg-Sr bulk scaffolds after 24 h cell culture with MC3T3-E1 corresponds with fluorescent microscopy images. Addition of Mg and Sr results in slower dissolution rate of B12.5-Mg-Sr glass as can be seen from B and Si release profiles. Precipitation of Ca and P into a probably HA-like layer indicates bioactivity of these glass compositions. Longer preincubation time does not affect ion release from B12.5-Mg-Sr scaffolds. However, it decreases Si^{4+}, B^{3+} and P^{3-} ion release from B12.5, which could explain why longer preincubation with B12.5 results in better cell survival. However, longer preincubation did not affect cell survival with B12.5-Mg-Sr scaffolds.

3.2.3. Effect of scaffolds manufacturing method on cell survival and ion release

Human ADSC were used to evaluate how different scaffolds manufacturing methods affected the cell survival. These cells, show greater translational potential which make them more clinically relevant compared to animal derived cells. With murine MC3T3-E1 cells, it was observed that all scaffolds made from B12.5-Mg-Sr glass composition seemed to provide better cell survival than B12.5 glass composition, hence only the former composition was utilized in the following experiments.

The Fig. 17 shows fluorescent microscope images of viable and necrotic cells after 1,3 and 7 days of culture with bulk, burn-off and 3D printed B12.5-Mg-Sr scaffolds. Moreover, based on preincubation results, preincubation of 2 days in TRIS and 24 h in αMEM was used. The cell density increased throughout the seven days of culturing, and there was no significant difference between the studied scaffold types (burn-off vs 3D printed). Scaffolds presence did not prevent the survival of the cells around it (Fig. 17a-l). On all the scaffolds tops, there is comparable number of alive cells (Fig. 17A-I). Only after 7 days of cell culture there was significantly more cells on the top of the bulk, than on other scaffolds. Moreover, cell migration inside the 3D printed scaffolds could also be observed. However, this was observed only beneath the top layer as imaging along the z-axis was limited.

Despite 3D printed scaffolds higher porosity, surface area and ion release concentrations, cell viability is comparable with positive control and other scaffold types. This indicates that B12.5-Mg-Sr glass composition is a promising candidate for 3D printing scaffolds with interconnected porosity. However, this result should be further confirmed by studying the proliferation of the cells more deeply.

Next, the ion concentrations in αMEM after cell culture were analyzed using ICP-OES (Fig. 18). Si^{4+} and B^{3+} ion release concentrations were increasing over course of cell culture (Fig. 18 a-b). Si^{4+} ion concentrations were not significantly different between scaffold types (Fig. 18a). 3D scaffolds produce higher B^{3+} ion concentration compared to bulk and burn-off scaffolds (Fig. 18b). These results indicate that 3D printed scaffolds dissolve faster, most probably due to their higher surface area connected with their high porosity.

It has been reported that B concentration of ≤ 0.65 mmol in the culture medium supports the proliferation and function of MLO-A5 cells (H. [53]. However, extensive B release, in vitro, has been shown to result in cells death [11]; H. [53]; Q. [12]. B concentrations above 0.65 mmol were shown to decrease the growth and proliferation rate of bone marrow cells (BMSc) (H. [53]. Similar results were reported by Brown et al. where B concentrations of 1.5 mmol in the culture medium inhibits cell proliferation [11]. In our study, the non-cumulative B concentration at each timepoint was always below 8 mmol/L. Nevertheless, despite potential cytotoxicity, B12.5-Mg-Sr scaffolds have been shown to support of hADSCs viability and proliferation.

Ca release was highest from 3D scaffolds and lowest from bulk scaffolds (Fig. 18c). P^{3-} ion concentrations are decreasing linearly, with lowest ion release from 3D scaffolds and highest ion release from bulk scaffolds (Fig. 18d). Ca and P consumption indicate Ca-P reactive layer deposition. Consumption was biggest for 3D printed scaffolds, most probably due to their higher dissolution rate. This leads to faster oversaturation of culture media with P^{3-} ions, and thus greater precipitation. Moreover, low concentration of Ca between 2 and 4 mmol has been shown to support osteoblast proliferation. Higher Ca concentration between 6 and 8 mmol has been shown to favor osteoblast differentiation and mineralization. Whereas Ca concentrations higher than 10 mmol were shown to be cytotoxic [55]. In our study, non-cumulative Ca concentration for all scaffold types were between 1.8 and 2.6 mmol and has also been shown to support hADSCs proliferation. Mg^{2+} and Sr^{2+} ion release (Fig. 18e-f) was highest from 3D printed scaffolds and lowest from bulk scaffolds.

Summarizing, 3D scaffolds release highest concentrations of B^{3+}, Ca^{2+}, Mg^{2+} and Sr^{2+} ions probably due to their highest porosity and surface area. However, these ion levels are low enough to provide cell survival comparable with other less porous scaffolds.

4. Conclusions

Bioactive borosilicate glass scaffolds, made from B12.5 and B12.5-Mg-Sr compositions, were successfully produced using heat sintering of packed particles to produce a “bulk” scaffold, 3D printing and porogen burn-off manufacturing methods. The consumption of P^{3-} and Ca^{2+}

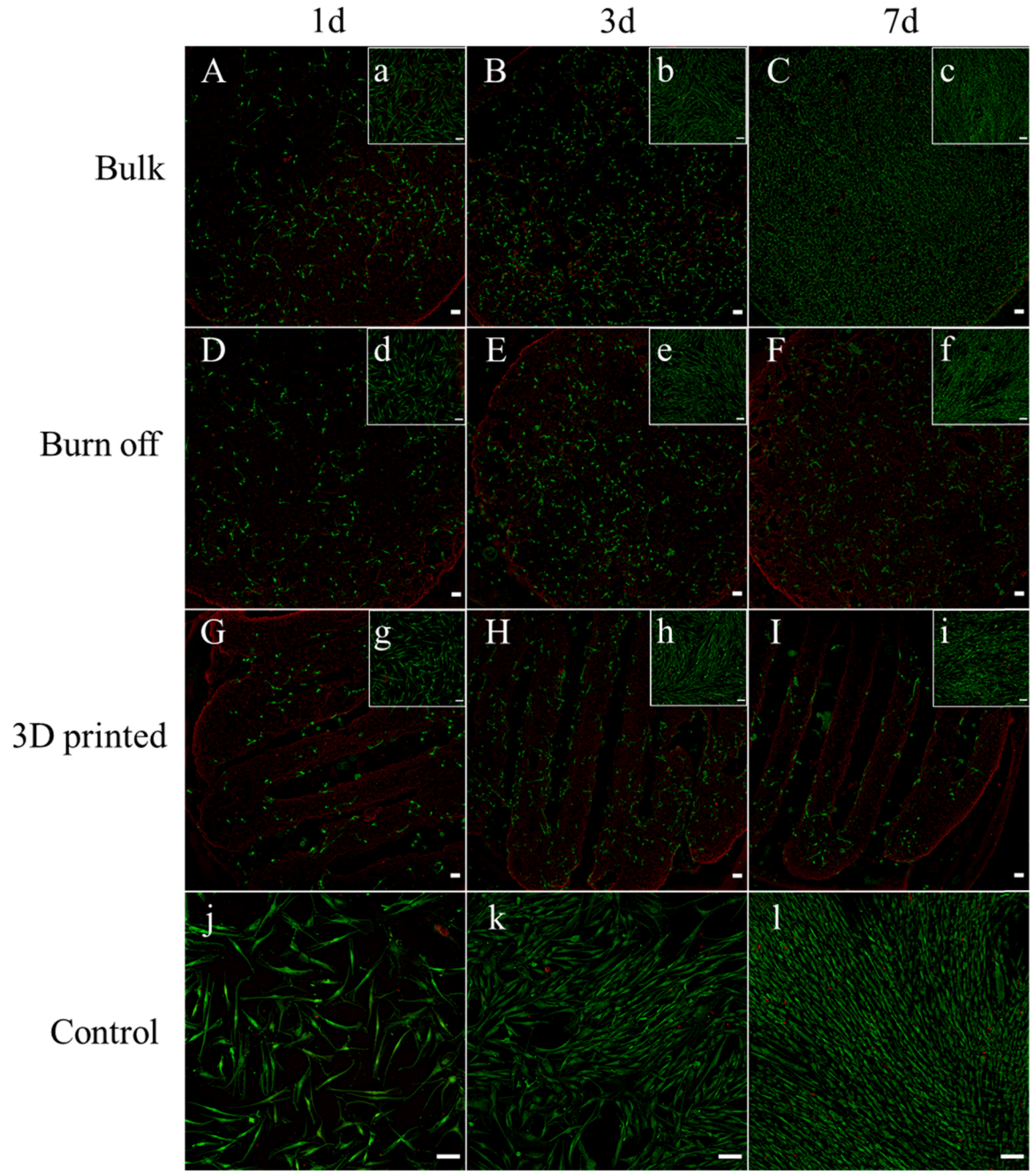

Fig. 17. Fluorescent images of hADSCs cells after 1,3 and 7 days of culture in αMEM culture medium. Images A-I show the top of bulk, burn-off and 3D printed scaffolds. Images a-l show the bottom of the wellplate. Viable (green) and necrotic (red) cells were stained with Calcein AM and Ethidium homodimer-1 respectively. Part of the red lines are product of autofluorescence from scaffolds. Scale bar 100 μm.

ions during immersion in SBF suggest the formation of a HA-like layer, indicating scaffolds bioactivity. Moreover, the studied 3D printed, and burn-off scaffolds met porosity and pore size requirements for favorable for bone tissue engineering applications. Moreover, the 3D printed scaffolds exhibited interconnected porosity, more homogenous pore sizes, and overall better reproducibility.

Scaffolds made from B12.5-Mg-Sr glass composition dissolved in TRIS and precipitated Ca and P in SBF in a slower way compared to B12.5 scaffolds. This could be attributed to stabilizing effect of MgO and SrO substitution for CaO on borate network. This had a significant effect on MC3T3-E1 cell survival and proliferation. It was shown that only B12.5-Mg-Sr glass composition supported cell survival. However, toxicity of B12.5 scaffolds due to high ion release, in static cell culture, could be resolved using dynamic cell culture.

Furthermore, 3D printed and burn-off scaffolds, with higher porosity compared to bulk scaffolds, exhibited faster dissolution in TRIS. These are attributed to greater surface area resulting from higher porosity. Most importantly, when hADSCs were cultured with B12.5-Mg-Sr bulk, burn-off and 3D printed scaffolds, cells survival was comparable to control cell culture without scaffolds. Thus, differences in dissolution and precipitation rate between these scaffolds were not significant. Moreover, migration of hADSCs beneath the top layer in the 3D printed scaffolds was also observed.

Additionally, preincubation of scaffolds in TRIS and αMEM was shown to be an effective way to decrease burst release of ions during cell culture with cells. Total preincubation period of 3 days was chosen to be

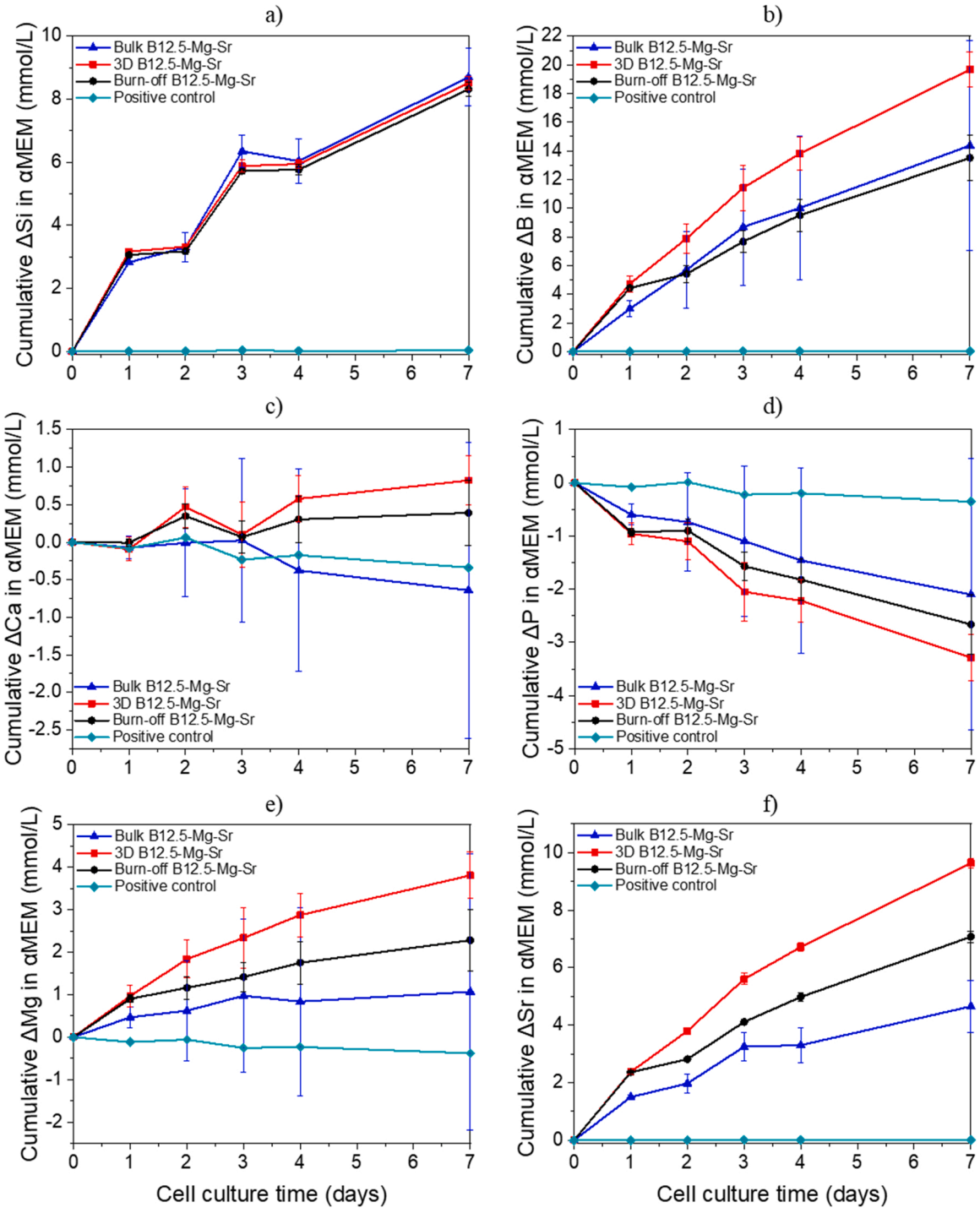

Fig. 18. Concentrations of a-f) Si, B, Ca, P, Mg and Sr in αMEM culture medium after 1, 3 and 7 days of hADSCs culture with Bulk, Burn-off and 3D printed B12.5-Mg-Sr scaffolds as a function of time. ΔElement = [Element] in αMEM in the presence of the sample – [Element] in αMEM initial solution.

optimal.

3D printed scaffolds made from B12.5-Mg-Sr glass composition were developed to be bioactive, with high interconnected porosity with good pore size and optimal dissolution rate, allowing better hADSCs cell survival. The B12.5-Mg-Sr 3D printed scaffolds met the requirements of the structural properties and reproducibility. Based on these results, the future research will be focused on 3D printed B12.5-Mg-Sr scaffolds. To further improve the properties and functionality of these constructs, they could be combined for example with a cellularized collagen gel to produce a hybrid scaffold. Additionally, the ability of hADSCs to differentiate towards osteogenic lineage when cultured with hybrid scaffolds will be studied.

CRediT authorship contribution statement

Agata Szczodra: Conceptualization, Methodology, Validation, Formal analysis, Investigation, Data curation, Writing – original draft, Visualization **Jenna M. Tainio**: Conceptualization, Methodology, Validation, Writing – review & editing **Amel Houaoui**: Conceptualization, Methodology, Validation, Formal analysis, Investigation, Data curation, Writing – original draft, Writing – review & editing, Visualization **Hongfei Liu:** Methodology, Validation, Formal analysis, Investigation,

Data curation, Writing – review & editing, Visualization **Juuso Pohjola:** Conceptualization, Methodology, Validation, Formal analysis, Investigation, Data curation **Susanna Miettinen:** Conceptualization, Methodology, Validation, Resources, Writing – review & editing ***Delia S. Brauer:*** Conceptualization, Methodology, Validation, Writing – review & editing, Project administration, Funding acquisition **J. Massera:** Conceptualization, Methodology, Validation, Resources, Writing – original draft, Writing – review & editing, Supervision, Project administration, Funding acquisition.

Declaration of Competing Interest

The authors declare the following financial interests/personal relationships which may be considered as potential competing interests: Agata Szczodra, Jonathan Massera reports financial support was provided by Academy of Finland. Jenna Tainio, Juuso Pohjola reports financial support was provided by German Academic Exchange Service.

Data Availability

Data will be made available on request.

Acknowledgments

Authors would like to thank the Academy of Finland (research grant #331924) for financial support of the AS as well as the DAAD-Finland mobility program (grant #295962) for the mobility of JT and JP to Jena university.

Appendix A. Supporting information

Supplementary data associated with this article can be found in the online version at doi:10.1016/j.mtcomm.2023.105984.

References

[1] M. Brink, The influence of alkali and alkaline earths on the working range for bioactive glasses, J. Biomed. Mater. Res. 36 (1) (1997) 109–117, https://doi.org/10.1002/(SICI)1097-4636(199707)36:1<109::AID-JBM13>3.0.CO;2-D.
[2] S. Fagerlund, J. Massera, M. Hupa, L. Hupa, T–T–T behaviour of bioactive glasses 1–98 and 13–93, J. Eur. Ceram. Soc. 32 (11) (2012) 2731–2738, https://doi.org/10.1016/j.jeurceramsoc.2011.10.040.
[3] J. Massera, S. Fagerlund, L. Hupa, M. Hupa, Crystallization mechanism of the bioactive glasses, 45S5 and S53P4, J. Am. Ceram. Soc. 95 (2) (2012) 607–613, https://doi.org/10.1111/j.1551-2916.2011.05012.x.
[4] M.N. Rahaman, D.E. Day, B. Sonny Bal, Q. Fu, S.B. Jung, L.F. Bonewald, A. P. Tomsia, Bioactive glass in tissue engineering, Acta Biomater. 7 (6) (2011) 2355–2373, https://doi.org/10.1016/j.actbio.2011.03.016.
[5] L.-C. Gerhardt, A.R. Boccaccini, Bioactive glass and glass-ceramic scaffolds for bone tissue engineering, Materials 3 (7) (2010) 3867–3910, https://doi.org/10.3390/ma3073867.
[6] H. Jodati, B. Yılmaz, Z. Evis, A review of bioceramic porous scaffolds for hard tissue applications: effects of structural features, Ceram. Int. 46 (10) (2020) 15725–15739, https://doi.org/10.1016/j.ceramint.2020.03.192.
[7] V. Karageorgiou, D. Kaplan, Porosity of 3D biomaterial scaffolds and osteogenesis, Biomaterials 26 (27) (2005) 5474–5491, https://doi.org/10.1016/j.biomaterials.2005.02.002.
[8] A. Yao, D. Wang, W. Huang, Q. Fu, M.N. Rahaman, D.E. Day, In vitro bioactive characteristics of borate-based glasses with controllable degradation behavior, J. Am. Ceram. Soc. 90 (1) (2007) 303–306, https://doi.org/10.1111/j.1551-2916.2006.01358.x.
[9] M. Fabert, N. Ojha, E. Erasmus, M. Hannula, M. Hokka, J. Hyttinen, J. Rocherullé, I. Sigalas, J. Massera, Crystallization and sintering of borosilicate bioactive glasses for application in tissue engineering, J. Mater. Chem. B 5 (23) (2017) 4514–4525, https://doi.org/10.1039/C7TB00106A.
[10] W. Huang, D.E. Day, K. Kittiratanapiboon, M.N. Rahaman, Kinetics and mechanisms of the conversion of silicate (45S5), borate, and borosilicate glasses to hydroxyapatite in dilute phosphate solutions, J. Mater. Sci.: Mater. Med. 17 (7) (2006) 583–596, https://doi.org/10.1007/s10856-006-9220-z.
[11] R.F. Brown, M.N. Rahaman, A.B. Dwilewicz, W. Huang, D.E. Day, Y. Li, B.S. Bal, Effect of borate glass composition on its conversion to hydroxyapatite and on the proliferation of MC3T3-E1 cells, J. Biomed. Mater. Res. Part A 88A (2) (2009) 392–400, https://doi.org/10.1002/jbm.a.31679.
[12] Q. Fu, M.N. Rahaman, B.S. Bal, L.F. Bonewald, K. Kuroki, R.F. Brown, Silicate, borosilicate, and borate bioactive glass scaffolds with controllable degradation rate for bone tissue engineering applications. II. In vitro and in vivo biological evaluation, J. Biomed. Mater. Res. Part A 95A (1) (2010) 172–179, https://doi.org/10.1002/jbm.a.32823.
[13] Narayan, R., Colombo, P., Halbig, M., & Mathur, S. (Eds.). (2012). *A*dvances in Bioceramics and Porous Ceramics V. John Wiley & Sons, Inc. https://doi.org/10.1002/9781118217504.
[14] J.M. Tainio, D.A.A. Salazar, A. Nommeots-Nomm, C. Roiland, B. Bureau, D. R. Neuville, D.S. Brauer, J. Massera, Structure and in vitro dissolution of Mg and Sr containing borosilicate bioactive glasses for bone tissue engineering, J. Non-Cryst. Solids 533 (2020), 119893, https://doi.org/10.1016/j.jnoncrysol.2020.119893.
[15] J. Massera, L. Hupa, Influence of SrO substitution for CaO on the properties of bioactive glass S53P4, J. Mater. Sci.: Mater. Med. 25 (3) (2014) 657–668, https://doi.org/10.1007/s10856-013-5120-1.
[16] J. Massera, L. Hupa, M. Hupa, Influence of the partial substitution of CaO with MgO on the thermal properties and in vitro reactivity of the bioactive glass S53P4, J. Non-Cryst. Solids 358 (18–19) (2012) 2701–2707, https://doi.org/10.1016/j.jnoncrysol.2012.06.032.
[17] P. Naruphontjirakul, O. Tsigkou, S. Li, A.E. Porter, J.R. Jones, Human mesenchymal stem cells differentiate into an osteogenic lineage in presence of strontium containing bioactive glass nanoparticles, Acta Biomater. 90 (2019) 373–392, https://doi.org/10.1016/j.actbio.2019.03.038.
[18] M.E. Santocildes-Romero, A. Crawford, P. v Hatton, R.L. Goodchild, I.M. Reaney, C.A. Miller, The osteogenic response of mesenchymal stromal cells to strontium-substituted bioactive glasses, J. Tissue Eng. Regen. Med. 9 (5) (2015) 619–631, https://doi.org/10.1002/term.2003.
[19] J. Liu, S.C.F. Rawlinson, R.G. Hill, F. Fortune, Strontium-substituted bioactive glasses in vitro osteogenic and antibacterial effects, Dent. Mater. 32 (3) (2016) 412–422, https://doi.org/10.1016/j.dental.2015.12.013.
[20] P. Naruphontjirakul, A.E. Porter, J.R. Jones, In vitro osteogenesis by intracellular uptake of strontium containing bioactive glass nanoparticles, Acta Biomater. 66 (2018) 67–80, https://doi.org/10.1016/j.actbio.2017.11.008.
[21] S. Hesaraki, M. Alizadeh, H. Nazarian, D. Sharifi, Physico-chemical and in vitro biological evaluation of strontium/calcium silicophosphate glass, J. Mater. Sci. Mater. Med. 21 (2) (2010) 695–705, https://doi.org/10.1007/s10856-009-3920-0.
[22] A. Hoppe, B. Sarker, R. Detsch, N. Hild, D. Mohn, W.J. Stark, A.R. Boccaccini, In vitro reactivity of Sr-containing bioactive glass (type 1393) nanoparticles, J. Non-Cryst. Solids (2014), https://doi.org/10.1016/j.jnoncrysol.2013.12.010.
[23] L. Hupa, S. Fagerlund, J. Massera, L. Björkvik, Dissolution behavior of the bioactive glass S53P4 when sodium is replaced by potassium, and calcium with magnesium or strontium, J. Non-Cryst. Solids 432 (2016) 41–46, https://doi.org/10.1016/j.jnoncrysol.2015.03.026.
[24] Ż. Ciosek, K. Kot, D. Kosik-Bogacka, N. Łanocha-Arendarczyk, I. Rotter, The effects of calcium, magnesium, phosphorus, fluoride, and lead on bone tissue, Biomolecules 11 (4) (2021) 506, https://doi.org/10.3390/biom11040506.
[25] L.Y. He, X.M. Zhang, B. Liu, Y. Tian, W.H. Ma, Effect of magnesium ion on human osteoblast activity, Braz. J. Med. Biol. Res. 49 (7) (2016), https://doi.org/10.1590/1414-431×20165257.
[26] S. Bose, S. Tarafder, S.S. Banerjee, N.M. Davies, A. Bandyopadhyay, Understanding in vivo response and mechanical property variation in MgO, SrO and SiO2 doped β-TCP, Bone 48 (6) (2011) 1282–1290, https://doi.org/10.1016/j.bone.2011.03.685.
[27] Q. Fu, M.N. Rahaman, H. Fu, X. Liu, Silicate, borosilicate, and borate bioactive glass scaffolds with controllable degradation rate for bone tissue engineering applications. I. Preparation and in vitro degradation, J. Biomed. Mater. Res. Part A 95A (1) (2010) 164–171, https://doi.org/10.1002/jbm.a.32824.
[28] D. Ke, S. Tarafder, S. Vahabzadeh, S. Bose, Effects of MgO, ZnO, SrO, and SiO2 in tricalcium phosphate scaffolds on in vitro gene expression and in vivo osteogenesis, Mater. Sci. Eng.: C. 96 (2019) 10–19, https://doi.org/10.1016/j.msec.2018.10.073.
[29] F. Baino, E. Fiume, J. Barberi, S. Kargozar, J. Marchi, J. Massera, E. Verné, Processing methods for making porous bioactive glass-based scaffolds—a state-of-the-art review, Int. J. Appl. Ceram. Technol. 16 (5) (2019) 1762–1796, https://doi.org/10.1111/ijac.13195.
[30] Y. Niu, L. Guo, J. Liu, H. Shen, J. Su, X. An, B. Yu, J. Wei, J.-W. Shin, H. Guo, F. Ji, D. He, Bioactive and degradable scaffolds of the mesoporous bioglass and poly(<scp>l</scp> -lactide) composite for bone tissue regeneration, J. Mater. Chem. B 3 (15) (2015) 2962–2970, https://doi.org/10.1039/C4TB01796J.
[31] K. Rezwan, Q.Z. Chen, J.J. Blaker, A.R. Boccaccini, Biodegradable and bioactive porous polymer/inorganic composite scaffolds for bone tissue engineering, Biomaterials 27 (18) (2006) 3413–3431, https://doi.org/10.1016/j.biomaterials.2006.01.039.
[32] D.W. Hutmacher, S. Cool, Concepts of scaffold-based tissue engineering—the rationale to use solid free-form fabrication techniques, J. Cell. Mol. Med. 11 (4) (2007) 654–669, https://doi.org/10.1111/j.1582-4934.2007.00078.x.
[33] C. Shuai, W. Yang, P. Feng, S. Peng, H. Pan, Accelerated degradation of HAP/PLLA bone scaffold by PGA blending facilitates bioactivity and osteoconductivity, Bioact. Mater. 6 (2) (2021) 490–502, https://doi.org/10.1016/j.bioactmat.2020.09.001.
[34] S. Fagerlund, L. Hupa, M. Hupa, Dissolution patterns of biocompatible glasses in 2-amino-2-hydroxymethyl-propane-1,3-diol (Tris) buffer, Acta Biomater. 9 (2) (2013) 5400–5410, https://doi.org/10.1016/j.actbio.2012.08.051.
[35] L. Kyllönen, S. Haimi, B. Mannerström, H. Huhtala, K.M. Rajala, H. Skottman, G. K. Sándor, S. Miettinen, Effects of different serum conditions on osteogenic differentiation of human adipose stem cells in vitro, Stem Cell Res. Ther. 4 (1) (2013) 17, https://doi.org/10.1186/scrt165.
[36] M. Patrikoski, M. Juntunen, S. Boucher, A. Campbell, M.C. Vemuri, B. Mannerström, S. Miettinen, Development of fully defined xeno-free culture

system for the preparation and propagation of cell therapy-compliant human adipose stem cells, Stem Cell Res. Ther. 4 (2) (2013) 27, https://doi.org/10.1186/scrt175.
[37] L. Hyväri, M. Ojansivu, M. Juntunen, K. Kartasalo, S. Miettinen, S. Vanhatupa, Focal adhesion kinase and ROCK signaling are switch-like regulators of human adipose stem cell differentiation towards osteogenic and adipogenic lineages, Stem Cells Int. 2018 (2018) 1–13, https://doi.org/10.1155/2018/2190657.
[38] P. Bourin, B.A. Bunnell, L. Casteilla, M. Dominici, A.J. Katz, K.L. March, H. Redl, J. P. Rubin, K. Yoshimura, J.M. Gimble, Stromal cells from the adipose tissue-derived stromal vascular fraction and culture expanded adipose tissue-derived stromal/stem cells: a joint statement of the International Federation for Adipose Therapeutics and Science (IFATS) and the International Society for Cellular Therapy (ISCT), Cytotherapy 15 (6) (2013) 641–648, https://doi.org/10.1016/j.jcyt.2013.02.006.
[39] M. Dominici, K. le Blanc, I. Mueller, I. Slaper-Cortenbach, F.C. Marini, D.S. Krause, R.J. Deans, A. Keating, D.J. Prockop, E.M. Horwitz, Minimal criteria for defining multipotent mesenchymal stromal cells. The International Society for Cellular Therapy position statement, Cytotherapy 8 (4) (2006) 315–317, https://doi.org/10.1080/14653240600855905.
[40] J. Ge, L. Guo, S. Wang, Y. Zhang, T. Cai, R.C.H. Zhao, Y. Wu, The size of mesenchymal stem cells is a significant cause of vascular obstructions and stroke, Stem Cell Rev. Rep. 10 (2) (2014) 295–303, https://doi.org/10.1007/s12015-013-9492-x.
[41] H. Sudo, H.A. Kodama, Y. Amagai, S. Yamamoto, S. Kasai, In vitro differentiation and calcification in a new clonal osteogenic cell line derived from newborn mouse calvaria, J. Cell Biol. 96 (1) (1983) 191–198, https://doi.org/10.1083/jcb.96.1.191.
[42] Iordache, F. (2019). Bioprinted scaffolds. In Materials for Biomedical Engineering (pp. 35–60). Elsevier. https://doi.org/10.1016/B978–0-12–816901-8.00002-X.
[43] M. Diba, F. Tapia, A.R. Boccaccini, L.A. Strobel, Magnesium-containing bioactive glasses for biomedical applications, Int. J. Appl. Glass Sci. 3 (3) (2012) 221–253, https://doi.org/10.1111/j.2041-1294.2012.00095.x.
[44] M.T. Souza, M.C. Crovace, C. Schröder, H. Eckert, O. Peitl, E.D. Zanotto, Effect of magnesium ion incorporation on the thermal stability, dissolution behavior and bioactivity in Bioglass-derived glasses, J. Non-Cryst. Solids 382 (2013) 57–65, https://doi.org/10.1016/j.jnoncrysol.2013.10.001.
[45] Q. Fu, E. Saiz, M.N. Rahaman, A.P. Tomsia, Bioactive glass scaffolds for bone tissue engineering: state of the art and future perspectives, Mater. Sci. Eng.: C. 31 (7) (2011) 1245–1256, https://doi.org/10.1016/j.msec.2011.04.022.
[46] X. Liu, M.N. Rahaman, G.E. Hilmas, B.S. Bal, Mechanical properties of bioactive glass (13-93) scaffolds fabricated by robotic deposition for structural bone repair, Acta Biomater. 9 (6) (2013) 7025–7034, https://doi.org/10.1016/j.actbio.2013.02.026.
[47] L. Olah, K. Filipczak, Z. Jaegermann, T. Czigany, L. Borbas, S. Sosnowski, P. Ulanski, J.M. Rosiak, Synthesis, structural and mechanical properties of porous polymeric scaffolds for bone tissue regeneration based on neat poly (ε-caprolactone) and its composites with calcium carbonate, Polym. Adv. Technol. 17 (11–12) (2006) 889–897, https://doi.org/10.1002/pat.768.
[48] A. Li, Y. Lv, H. Ren, Y. Cui, C. Wang, R.A. Martin, D. Qiu, In vitro evaluation of a novel pH neutral calcium phosphosilicate bioactive glass that does not require preconditioning prior to use, Int. J. Appl. Glass Sci. 8 (4) (2017) 403–411, https://doi.org/10.1111/ijag.12321.
[49] F.E. Ciraldo, E. Boccardi, V. Melli, F. Westhauser, A.R. Boccaccini, Tackling bioactive glass excessive in vitro bioreactivity: preconditioning approaches for cell culture tests, Acta Biomater. 75 (2018) 3–10, https://doi.org/10.1016/j.actbio.2018.05.019.
[50] J.R. Jones, Reprint of: Review of bioactive glass: from Hench to hybrids, Acta Biomater. 23 (2015) S53–S82, https://doi.org/10.1016/j.actbio.2015.07.019.
[51] M. Arango-Ospina, L. Hupa, A.R. Boccaccini, Bioactivity and dissolution behavior of boron-containing bioactive glasses under static and dynamic conditions in different media, Biomed. Glass 5 (1) (2019) 124–139, https://doi.org/10.1515/bglass-2019-0011.
[52] A. Rámila, M. Vallet-Regı, Static and dynamic in vitro study of a sol–gel glass bioactivity, Biomaterials 22 (16) (2001) 2301–2306, https://doi.org/10.1016/S0142-9612(00)00419-1.
[53] H. Fu, Q. Fu, N. Zhou, W. Huang, M.N. Rahaman, D. Wang, X. Liu, In vitro evaluation of borate-based bioactive glass scaffolds prepared by a polymer foam replication method, Mater. Sci. Eng.: C. 29 (7) (2009) 2275–2281, https://doi.org/10.1016/j.msec.2009.05.013.
[54] E. Gentleman, Y.C. Fredholm, G. Jell, N. Lotfibakhshaiesh, M.D. O'Donnell, R. G. Hill, M.M. Stevens, The effects of strontium-substituted bioactive glasses on osteoblasts and osteoclasts in vitro, Biomaterials 31 (14) (2010) 3949–3956, https://doi.org/10.1016/j.biomaterials.2010.01.121.
[55] S. Maeno, Y. Niki, H. Matsumoto, H. Morioka, T. Yatabe, A. Funayama, Y. Toyama, T. Taguchi, J. Tanaka, The effect of calcium ion concentration on osteoblast viability, proliferation and differentiation in monolayer and 3D culture, Biomaterials 26 (23) (2005) 4847–4855, https://doi.org/10.1016/j.biomaterials.2005.01.006.